SIMPLEST BIFURCATION DIAGRAMS FOR MONOTONE FAMILIES OF VECTOR FIELDS ON A TORUS

C.BAESENS AND R.S.MACKAY

Abstract. In Part 1 we prove that the bifurcation diagram for a monotone two-parameter family of vector fields on a torus has to be at least as complicated as the conjectured simplest one proposed in [BGKM1]. To achieve this we define "simplest" by minimising sequentially the numbers of equilibria, Bogdanov-Takens points, closed curves of centre and of neutral saddle, intersections of curves of centre and neutral saddle, Reeb components, other invariant annuli, arcs of rotational homoclinic bifurcation of horizontal homotopy type, necklace points, contractible periodic orbits, points of neutral horizontal homoclinic bifurcation and half-plane fan points. We obtain two types of simplest case, including that initially proposed.

In Part 2 we analyse the bifurcation diagram for an explicit monotone family of vector fields on a torus and prove that it has at most two equilibria, precisely four Bogdanov-Takens points, no closed curves of centre nor closed curves of neutral saddle, at most two Reeb components, precisely four arcs of rotational homoclinic connection of "horizontal" homotopy type, eight horizontal saddle-node loop points, two necklace points, four points of neutral horizontal homoclinic connection, and two half-plane fan points, and there is no simultaneous existence of centre and neutral saddle, nor contractible homoclinic connection to a neutral saddle. Furthermore we prove that all saddle-nodes, Bogdanov-Takens points, non-neutral and neutral horizontal homoclinic bifurcations are non-degenerate and the Hopf condition is satisfied for all centres. We also find it has four points of degenerate Hopf bifurcation. Thus it provides an example of a family satisfying all the assumptions of Part 1 except the one of at most one contractible periodic orbit.

0. Introduction

There is a large literature on the qualitative theory of flows on surfaces; see [AZ] and Ch.14 of [KH] for reviews. Yet the subject of global bifurcations in families of flows on a surface has received little attention since the pioneering work for the torus in section 4 of [BGKM1] and the short supplementary article [BGKM2].

In this paper we complete and extend the results of [BGKM2] on the bifurcation diagrams for families of vector fields on a torus. "Complete" means fleshing out arguments that were only sketched there, deriving constraints on how the various bifurcation curves can be arranged (which was not tackled there), deducing the "simplest" arrangements (one of which was conjectured in [BGKM1] but hitherto not proved), and analysing in detail the example studied numerically in [BGKM2]. "Extend" means allowing families of vector fields that are monotone in parameter, not just the special case of $\dot{\mathbf{x}} = \boldsymbol{\Omega} + \mathbf{g}(\mathbf{x})$.

Date: March 15, 2018.

2010 *Mathematics Subject Classification.* 37E35, 37Gxx.

Key words and phrases. bifurcation, vector field, torus, simplest.

We study two-parameter families of vector fields

$$\dot{\mathbf{x}} = G(\mathbf{\Omega}, \mathbf{x}) \tag{1}$$

with $\mathbf{x} \in \mathbb{T}^2 = \mathbb{R}^2/\mathbb{Z}^2$, $\mathbf{\Omega} \in \mathbb{R}^2$ and $G \in C^3$. We assume them to have monotone dependence on parameter $\mathbf{\Omega}$ in the sense that there is a positive constant c such that

$$\langle d_\Omega G\ \omega, \omega \rangle \geq c\ |\omega|^2 \tag{2}$$

for all tangent vectors ω to $\mathbb{R}^2$, where $d_\Omega G$ is the derivative of G with respect to $\mathbf{\Omega}$, $\langle \mathbf{\Omega}_1, \mathbf{\Omega}_2 \rangle = \mathbf{\Omega}_1^T B \mathbf{\Omega}_2$ is an inner product on $\mathbb{R}^2$ given by a constant positive-definite symmetric matrix B, and $|\omega| = \sqrt{\langle \omega, \omega \rangle}$. The results apply also to any family for which after a diffeomorphism on parameter space the dependence becomes monotone.

Our longer-term goal is to understand the bifurcation diagrams for generic monotone families of vector fields on the torus. By "generic" we mean that we consider a countable intersection of open dense subsets of C^3 families, chosen to restrict all their bifurcations to have codimension at most two and the families to be transverse to them.

In this paper we restrict attention to the simplest cases, defined by assuming genericity and applying the following criteria in sequence:

(1) minimise the maximum number of equilibria;
(2) minimise the number of B (Bogdanov-Takens) points;
(3) minimise the numbers of closed curves of centre[1] and of neutral saddle, and of intersections of arcs of centre and neutral saddle;
(4) minimise the number of invariant annuli (equivalently of periodic orbits) when there are no equilibria, or the more accessible surrogate of Reeb components;
(5) minimise the number of curves of rotational homoclinic connection of "horizontal" homotopy type;
(6) minimise the number of N (necklace) points;
(7) minimise the number of contractible periodic orbits or more accessible surrogates, including J points (contractible homoclinic connection to a neutral saddle) and intersections of curves of centre with contractible homoclinic connection;
(8) minimise the number of K points (neutral rotational homoclinic connection) of horizontal homotopy type;
(9) minimise the number of H points (half-plane fan).

Any other generic bifurcation diagrams have to be at least as complicated. As a result of our analysis we formulate throughout Part 1 a list of assumptions defining the simplest cases:

1: There are at most two equilibria;
2: There are at most four B points;
3a: There are no closed curves of centre nor closed curves of neutral saddle,
3b: There is no coexistence of centre and neutral saddle;
4a: There are at most two Reeb components for parameter values in the hole,
4b: There are no other invariant annuli for flows in the hole,
4c: There are no Reeb components outside the resonance region;

[1]Throughout the paper we use the term "centre" to refer to an equilibrium with purely imaginary complex conjugate eigenvalues. We do not imply the stronger meaning of an equilibrium with a neighbourhood foliated by periodic orbits.

5a: There are at most four Z points on the inner saddle-node curve,
5b: There are at most four Z points of horizontal homotopy types on the outer saddle-node curve,
5c: There are at most four curves of rotational homoclinic connection of horizontal homotopy types;
6: There are at most two necklace (N) points;
7a: There are no contractible homoclinic connections to a neutral saddle (J points),
7b: There is at most one contractible periodic orbit;
8: There are at most four K points for horizontal homotopy types;
9: There are at most two H points.

Our end result is that the simplest bifurcation diagrams are as in Figure 22, modulo orientations. The upper case there is that conjectured in Figure 6.5 of [BGKM1] supplemented by details for the half-plane fans described in other parts of [BGKM1]. The lower case is new, though similar.

For those unfamiliar with the above terms, we use much of the terminology of section 4 of [BGKM1], summarised here. A *B point* is a parameter value having an equilibrium with double eigenvalue 0 and non-diagonal Jordan normal form. A *Reeb component* for a two-dimensional vector field is an annulus bounded by periodic orbits in opposite directions and containing no equilibria nor other periodic orbits (this is a 2D analogue of the original notion of Reeb foliation of a solid torus). We use the term *rotational* as shorthand for "homotopically non-trivial". A *rotational homoclinic connection* (rhc) is a branch of stable manifold of a saddle connecting to a branch of unstable manifold of the same saddle but making a homotopically non-trivial loop; as the connection is broken a rotational periodic orbit is generated or destroyed, which is attracting or repelling according as the negative eigenvalue of the saddle is larger or smaller in magnitude than the positive eigenvalue. A *necklace point* (N) is a parameter point at which there are rhcs in opposite directions connecting the same saddle. A *J point* is a point of contractible homoclinic connection to a saddle at which the eigenvalues are equal and opposite ("neutral saddle"); a generic consequence is that a curve of saddle-node of contractible periodic orbit (csnp) emerges. A *K point* is a point of rotational homoclinic connection to a neutral saddle; a generic consequence is that a curve of rotational saddle-node periodic orbit (snp) emerges. An *H point* is an intersection of curves of rhc and snp in opposite directions. Basic results for flows on a torus are summarised in section 4 of [BGKM1]. The definition of "horizontal" homotopy type will be given in section 1.2.

In Part 2 we derive the bifurcation diagram for an explicit example:

$$\begin{aligned} \dot{x} &= \Omega_x - \cos 2\pi y - \varepsilon \cos 2\pi x \\ \dot{y} &= \Omega_y - \sin 2\pi y - \varepsilon \sin 2\pi x \end{aligned} \tag{3}$$

with ε small and positive, $\mathbf{x} = (x, y)$ on the torus $\mathbb{T}^2 = \mathbb{R}^2/\mathbb{Z}^2$, and parameters $\mathbf{\Omega} = (\Omega_x, \Omega_y) \in \mathbb{R}^2$ (equivalent to the example (28) of [BGKM2] under interchange of x and y). In the terminology of [G], it is a Mathieu family. We prove that it satisfies all but one (7b) of the assumptions above. Thus it demonstrates existence of a bifurcation diagram which is only slightly more complicated than what we believe to be the simplest possible ones derived in Part 1. Key to the analysis is a novel reversible approximation on a

cylinder, which is Hamiltonian on the universal cover but has attracting and repelling periodic orbits (section 2.8.1).

Part 1 was developed under the condition that all bifurcations are of codimension at most two and the family is transverse to them. This property is probably impossible to check for any example (there being infinitely many partial mode-locking tongues), but it is C^3-generic, so there are arbitrarily small perturbations of (3) in C^3 that satisfy this condition in addition. We check it here, however, for the principal features of the bifurcation diagram of (3) (saddle-node equilibria, Hopf bifurcation, Bogdanov-Takens points, and horizontal homoclinic connections).

1. Simplest bifurcation diagrams

1.1. **Minimising the maximum number of equilibria.** Let E be the set of equilibria in $\mathbb{R}^2 \times \mathbb{T}^2$, i.e. pairs $(\mathbf{\Omega}, \mathbf{x})$ where $G(\mathbf{\Omega}, \mathbf{x}) = 0$. Under the monotonicity assumption, E is the graph of a C^3 function $\mathbf{\Omega}^e : \mathbb{T}^2 \to \mathbb{R}^2$,

$$G(\mathbf{\Omega}^e(\mathbf{x}), \mathbf{x}) = \mathbf{0}, \tag{4}$$

as was proved in [KMG] for the analogous problem of fixed points of a monotone family of diffeomorphisms of the torus. The proof is that for each $\mathbf{x} \in \mathbb{T}^2$, the map $\mathbf{\Omega} \mapsto G(\mathbf{\Omega}, \mathbf{x})$ is a diffeomorphism of $\mathbb{R}^2$, because of the monotonicity of G with respect to Ω.

The *resonance region* for G is defined to be the set R of parameter values $\mathbf{\Omega}$ for which there exists an equilibrium. The resonance region R is the projection of E to $\mathbb{R}^2$.

As E is a graph over $\mathbb{T}^2$, it is non-empty, compact and connected, so R is non-empty, compact and connected. For a generic family the boundary of R consists of curves of generic saddle-node equilibrium (sne), connected at cusps (this is one place where we use $G \in C^3$) or transverse intersections of saddle-node curves. The number of equilibria increases by two on crossing a generic saddle-node curve, so every family has parameter values with at least two equilibria. Analysis in section 2.2 of the example (3) shows that it is possible to have no more than two equilibria.

Thus in our path towards the simplest bifurcation diagrams, we are led to make:

Assumption 1: There are at most two equilibria.

This implies that R is an annulus with generic saddle-node boundaries, as follows (the argument was given in [BGKM2]). Entering the region bounded by a cusp turns the number of equilibria locally from one to three so would imply parameter values with at least three equilibria (actually four because the total Poincaré index for a vector field on a torus is zero and generic equilibria have index ± 1), and a crossing of saddle-node curves generates a sector with at least four equilibria. Thus R is a compact connected set bounded by a finite number of closed curves of generic saddle-node and E is a double cover of the interior of R glued along the boundary. The surface E is orientable because it is a graph over $\mathbb{T}^2$. If R has N boundary components then E is an orientable surface of genus $N-1$. We know E is a torus, however, so has genus one. Therefore $N = 2$ and R is an annulus.

One of the two open annuli into which E is separated by the two closed curves of saddle-node consists of equilibria of index $+1$ (nodes, foci, improper nodes, centres). The other consists of equilibria of index -1 (saddles).

1.2. **The principal homotopy classes for a resonance.** The two boundary components of R divide E into two annuli (the two copies of R), so the saddle-node curves on E are two homotopically non-trivial curves on E. We choose to orient the saddle-node curves both anticlockwise on R. They are from the same primitive (i.e. not a multiple of any other) homotopy class on E, because one can be continuously deformed into the other. We denote by V the resulting homotopy class on $\mathbb{T}^2$. It can take any coprime rational direction in $\mathbb{R}^2/\mathbb{Z}^2$ (example (3) has $V = (1, 1)$).

A primitive closed path in E whose projection to R makes no revolutions around the hole corresponds to a different primitive homotopy class H from V. We choose to orient it to achieve anticlockwise rotation on the universal cover of $\mathbb{T}^2$ from H to V (example (3) has $H = (1, 0)$).

We can reduce to the case of V vertically upwards and H horizontally to the right by applying an invertible orientation-preserving linear coordinate change on the universal cover of $\mathbb{T}^2$: $\mathbf{x} = A\tilde{\mathbf{x}}$, where A is the matrix whose columns represent the homotopy types of H and V respectively. To preserve monotonicity of the parameter-dependence, we apply the parameter-change $\mathbf{\Omega} = A\tilde{\mathbf{\Omega}}$, and we make the associated change of the matrix B representing the inner product to $\tilde{B} = A^T BA$. To see monotonicity is preserved by these changes, note that $\dot{\tilde{\mathbf{x}}} = A^{-1}G(\mathbf{\Omega}, \mathbf{x})$, so the transformed family of vector fields is $\tilde{G}(\tilde{\mathbf{\Omega}}, \tilde{\mathbf{x}}) = A^{-1}G(A\tilde{\mathbf{\Omega}}, A\tilde{\mathbf{x}})$. Thus $d_{\tilde{\Omega}}\tilde{G} = A^{-1}\ d_\Omega G\ A$, and for any $\tilde{\omega} \in \mathbb{R}^2$,

$$(d_{\tilde{\Omega}}\tilde{G}\ \tilde{\omega})^T \tilde{B}\tilde{\omega} = \tilde{\omega}^T A^T d_\Omega G^T BA\tilde{\omega} \geq c\ (A\tilde{\omega})^T B(A\tilde{\omega}) = c\ \tilde{\omega}^T \tilde{B}\tilde{\omega}. \tag{5}$$

Thus in our pictures we draw V vertically upwards and H horizontally to the right (Figure 1), and we define $\pm H$ to be *horizontal* homotopy types.

1.3. **Orientation of $\mathbf{\Omega}^e$.** Next we discuss how the map $\mathbf{\Omega}^e$ defined by (4) treats orientation of area.

We endow E with the orientation inherited from $dx_1 \wedge dx_2$ on $\mathbb{T}^2$ as a graph over $\mathbb{T}^2$. The two copies of the interior of R have equilibria of opposite index, because the index changes at saddle-node curves and is constant on the components of the complement. The copy with index $+1$ inherits positive orientation in parameter space from E whereas the copy with index -1 inherits negative orientation.

One way to see this is that differentiating (4) implies

$$d_\Omega G\ d_x\Omega^e = -d_x G \tag{6}$$

on E, but by monotonicity, $d_\Omega G$ preserves orientation of area, while $d_x G$ preserves/reverses orientation according to the sign of the index (as $\mathbb{T}^2$ has even dimension the minus sign in (6) does not change orientation of area).

1.4. **B points.** Here we prove there are at least two B points on each of the saddle-node curves and at least two arcs of centre and two arcs of neutral saddle from them. The argument is analogous to that in [KMG] for discrete time.

Follow either of the saddle-node curves positively for a full revolution as shown in Figure 2(a) for the inner one. A non-zero tangent vector to the curve on E can be projected to both parameter and state space. Its component $\delta\mathbf{\Omega}$ on parameter space is non-zero because we assumed generic saddle-node curves. It makes one positive revolution. The component $\delta\mathbf{x}$ on the torus is also non-zero because E is a graph over $\mathbb{T}^2$, but it makes no revolutions because it is tangent to a curve of the non-trivial homotopy class V.

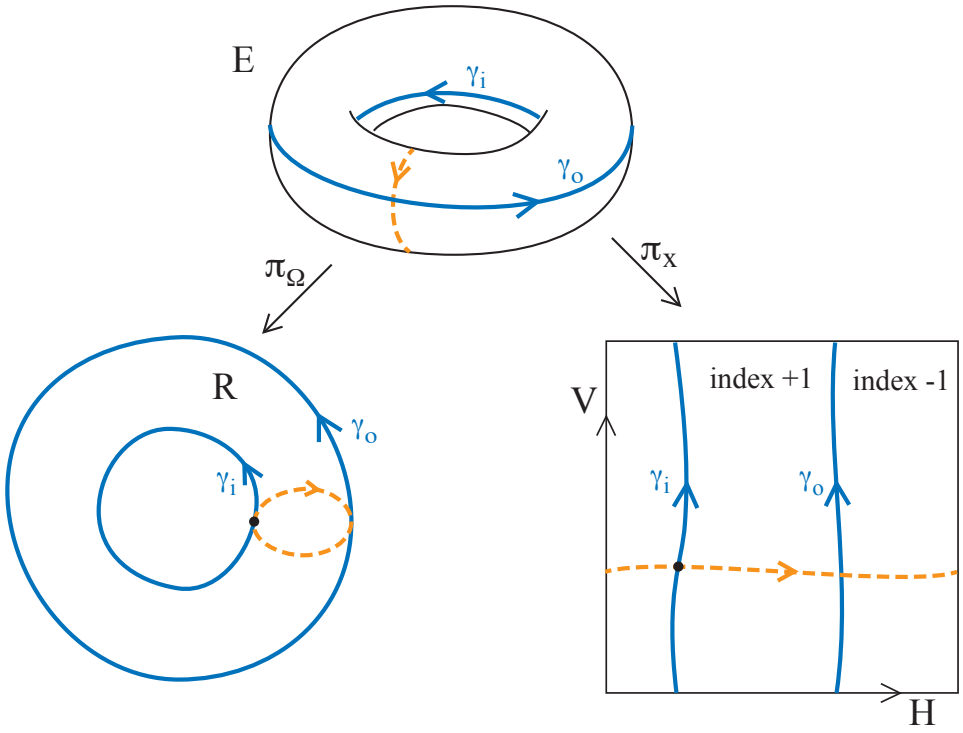

FIGURE 1. Projections of the set E of equilibria in $\mathbb{R}^2 \times \mathbb{T}^2$, π_Ω to parameter space $\mathbb{R}^2$, where it gives a double cover of an annulus R glued along their inner boundaries γ_i and along their outer boundaries γ_o, corresponding to saddle-node equilibria, and π_x to state space $\mathbb{T}^2$, represented as $\mathbb{R}^2/\mathbb{Z}^2$, using the choice of coordinates described in section 1.2. The dashed curve is a representative of the horizontal homotopy type H. The equilibria have index ± 1 in the regions indicated, corresponding to the discussion in section 1.3.

The kernel K of $d_x G$ is one-dimensional all along the saddle-node curve, by genericity of the saddle-nodes. From (6), the components $(\delta\mathbf{\Omega}, \delta\mathbf{x})$ are related by the equation

$$d_\Omega G \; \delta\mathbf{\Omega} = -d_x G \; \delta\mathbf{x}. \tag{7}$$

By monotonicity, $d_\Omega G$ is invertible so

$$\delta\mathbf{x}' := d_x G \; \delta\mathbf{x}$$

is never zero. Thus $\delta\mathbf{x}$ is never in K and, as they lie in two dimensions, K makes no revolutions either.

By monotonicity of G, $d_\Omega G \; \delta\mathbf{\Omega}$ makes one revolution, so it must lie in K at least twice. Thus $\delta\mathbf{x}'$ lies in K at least twice, as illustrated in Figure 2(b). This implies that $d_x G$ has double eigenvalue zero there with non-diagonal Jordan normal form, giving a Bogdanov-Takens point (B point). Note that every B point must arise from $\delta\mathbf{x}'$ falling in K because if there is any vector not in K that is mapped into K then all are.

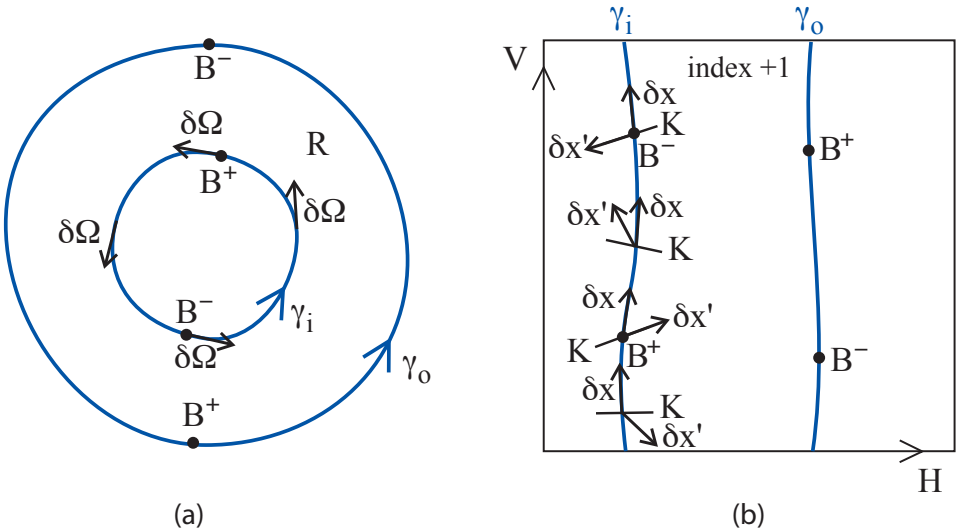

FIGURE 2. Illustration for the inner saddle-node curve of the proof that there are at least two B points on each saddle-node curve: (a) parameter space, (b) state space. The indices on the B points indicate Fiedler's B-index as in section 1.5.

Thus we have deduced there are at least two B points on each of the inner and outer saddle-node curves. Our example shows that it is possible to have precisely two on each (section 2.4), so our next condition for "simplest" is

Assumption 2: There are no more than four B points.

Following the choice of [GH], the family of vector fields in a neighbourhood of a B point can generically be written in the normal form

$$\begin{aligned} \dot{y}_1 &= y_2 + O(|y|^3) \\ \dot{y}_2 &= \varepsilon_1 + \varepsilon_2 y_1 + y_1^2 + \beta y_1 y_2 + O(|y|^3), \end{aligned} \tag{8}$$

with suitable new coordinates y_j and parameters ε_j, and $\beta \in \{\pm 1\}$. The bifurcation diagram for a generic B point is recalled in Figure 3. Tangent to the saddle-node curve at a generic B point is a curve of parameter values with an equilibrium of trace-zero. The equilibrium is a centre one way along this curve from B and a neutral saddle the other way. Generically, crossing a curve of centres produces a Hopf bifurcation of a contractible periodic orbit around the equilibrium. Near a generic B point, the direction of creation of the periodic orbit is always away from the saddle-node curve. There is also a half-curve of contractible homoclinic bifurcation coming out of the B point tangent to the saddle-node and Hopf curves in the same direction as the Hopf curve, which absorbs the contractible periodic orbit created by the Hopf bifurcation. An additional feature of a B point, which counts as a bifurcation in only a finer sense, is a curve of improper nodes, tangent between the saddle-node and trace-zero curves, separating nodes from foci.

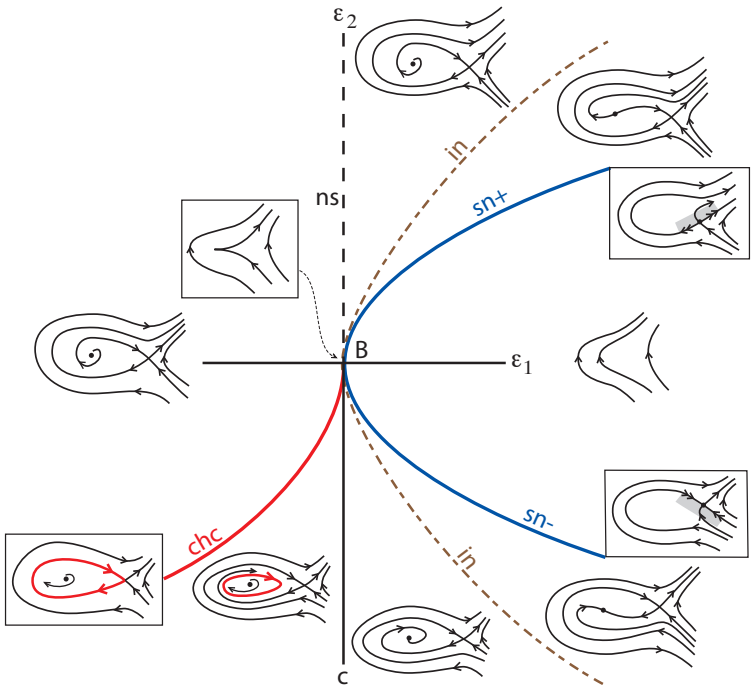

FIGURE 3. Unfolding of a B point, case $\beta = -1$ (the case $\beta = +1$ is given by reversing time and y_2). $sn\pm$ form a curve of saddle-node of equilibria, the vertical axis is a curve of tr $= 0$ with neutral saddle (ns) upwards (dashed) and centre (c, Hopf bifurcation) downwards, chc is a curve of contractible homoclinic connection, and in is a curve of improper node.

1.5. **Trace-zero curves.** A generic B point lies on a local curve of trace-zero in parameter space. Here we investigate the possibilities for the global picture of trace-zero curves.

1.5.1. *Introduction.* Generically, the set of parameter values with a trace-zero equilibrium is a union of smooth arcs, because if the parameter-derivative of the trace at a non-degenerate (meaning no eigenvalue 0) equilibrium is non-zero then locally in the product of state and parameter space the set is a smooth curve by the implicit function theorem, and zero parameter-derivative at a trace-zero point is codimension-three so does not occur generically. As a consequence, a curve of centres is generically a curve of Hopf bifurcation (the Hopf condition being that the trace vary at non-zero rate transversely), so we will use "centre" and "Hopf bifurcation" interchangeably. At a degenerate equilibrium with trace zero, the theory of B points gives a smooth arc of trace zero too, as in the previous section.

As a codimension-two phenomenon one can have degenerate Hopf bifurcation (D points of [BGKM1]), where the combination of Taylor coefficients that decides the direction of generation of a periodic orbit reverses, and this creates an arc of saddle-node of periodic orbits (note that "degenerate Hopf" does not imply "degenerate equilibrium").

Trace-zero curves either connect B points or form closed curves of only centre or only neutral saddle, avoiding the saddle-node curves. Closed curves of only centre or only neutral saddle do not occur in our example (section 2.4), so we will declare such cases not simplest.

Assumption 3a: There are no closed curves of only centre or only neutral saddle.

There are constraints on how the arcs of centre and neutral saddle can join up. One simple constraint is that two generic centre curves do not cross, because we have only one index +1 equilibrium. The same applies to two generic neutral saddle curves. Centre curves can cross neutral saddle curves, because they involve different equilibria, but such intersections introduce other complications (section 1.10), so in section 1.5.4 we will declare them not simplest.

1.5.2. *Fiedler's B-index.* A more subtle constraint is that Fiedler showed B points have a "B-index" ± 1 and that a curve of centres from a B point must end on a B point of the opposite B-index [F]. In our two-dimensional context, Fiedler's B-index is just the product of the coefficient β of (8) with the sign of the determinant of the mapping from parameter space to the normal form parameters $(\varepsilon_1, \varepsilon_2)$ [F]. If we orient the kernel K, then our proof of existence of B points in section 1.4 gives on each saddle-node curve existence of B points with $\delta\mathbf{x}'$ in the positive half of K and B points with $\delta\mathbf{x}'$ in the negative half of K. Choosing to orient K towards the side with equilibria of Poincaré index +1, the sign corresponds to Fiedler's B-index. To see this, Fiedler [F] gave an alternative characterisation of β as the sign of the rotation in parameter space from the side with two extra equilibria to the direction along the saddle-node curve to positive trace (in this two-dimensional context). Thus the B-indices of B points alternate along a curve of saddle-node bifurcation and we have precisely one of each on each of the two saddle-node curves. We label B points as $B^{\pm}$ according to their B-index.

1.5.3. *Curves of Hopf bifurcation.* It could be that a curve of Hopf bifurcation joins B points of opposite B-index on the same saddle-node curve, but we will prove in this subsection and Appendix A that there are at least two curves of Hopf bifurcation that connect B points on opposite saddle-node curves. Under Assumption 2 this uses up all the B points, so all the Hopf curves from B points join the two boundaries.

Our proof is by extending the idea of proof of existence of B points (section 1.4) into the index +1 region of E. Choose a foliation of R by circles homotopic to the boundaries of R and a transverse foliation by curves connecting the boundaries. Lifting to the part of E with index +1 equilibria, we obtain a foliation of an annulus in $\mathbb{T}^2$ with vertical leaves including the boundaries and a transverse foliation with horizontal leaves. See figure 4(a),(b). Note that the horizontal leaves meet the sne curves tangent to the kernel K of d_xG, because any other direction in state space is mapped by $\mathbf{\Omega}^e$ tangent to the sne curves in parameter space.

Denote an upward tangent to the vertical leaves by $\mathbf{v}$, its corresponding tangent in parameter space by ω, and a rightward tangent to the horizontal leaves by $\mathbf{h}$. Then $(\mathbf{h}, \mathbf{v})$ form a positively oriented frame for the tangent space to $\mathbb{T}^2$. As one moves up

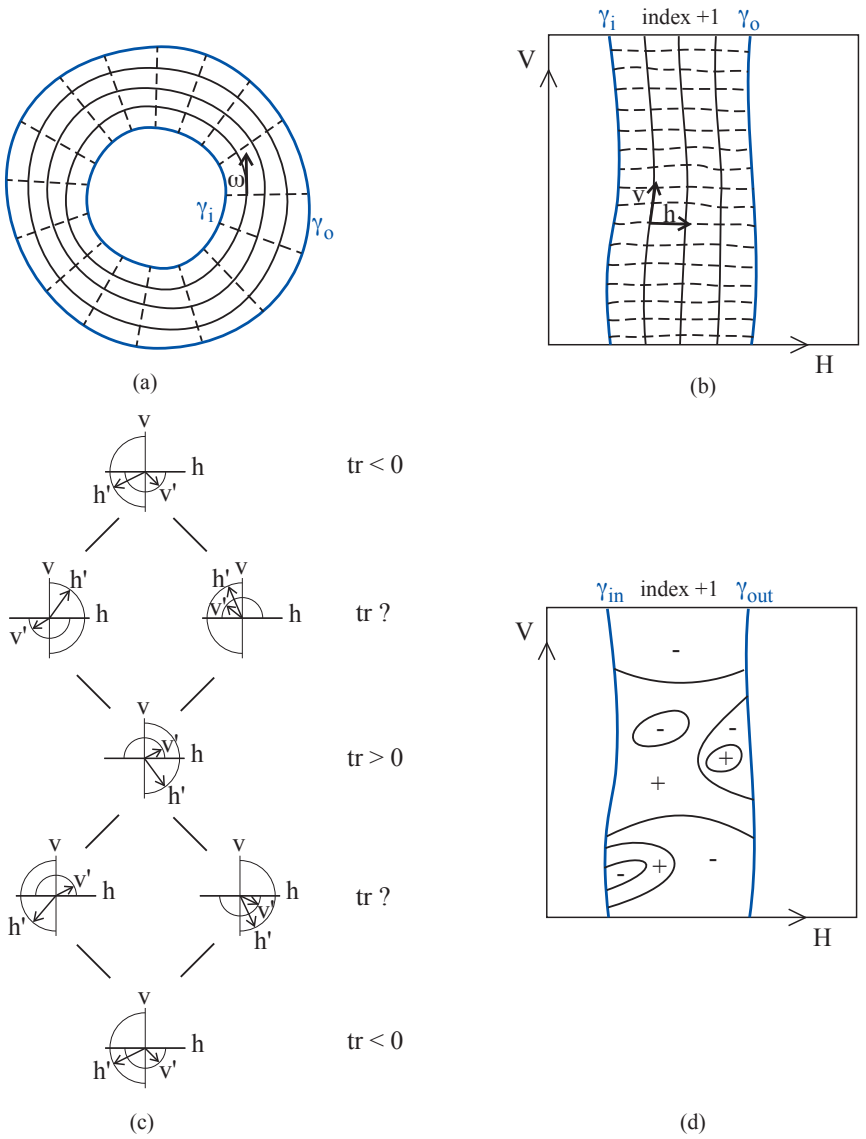

FIGURE 4. Illustration of the proof of existence of two curves of Hopf bifurcation connecting opposite saddle-node curves: (a) foliation in parameter space, (b) the index +1 region in state space, (c) obligation to pass through both signs of trace in one revolution, (d) resulting curves of trace-zero must include two crossing arcs as proved in Appendix A.

the annulus by one rotation, $(\mathbf{h}, \mathbf{v})$ makes no revolutions. In contrast, the vector

$$\mathbf{v}' := d_x G\ \mathbf{v} = -d_\Omega G\ \omega$$

is non-zero (by invertibility of d_xG off the boundaries of R) and performs one revolution, because ω does and $d_\Omega G$ is monotone. Then

$$\mathbf{h}' := d_xG\ \mathbf{h}$$

follows suit because again d_xG is invertible away from the boundaries. The frame $(\mathbf{h}', \mathbf{v}')$ is positively oriented because d_xG preserves orientation for index $+1$ points. The trace of d_xG is given by the sum of the component of $\mathbf{v}'$ in direction $\mathbf{v}$ and the component of $\mathbf{h}'$ in direction $\mathbf{h}$, with respect to the basis $(\mathbf{h}, \mathbf{v})$. Referring to Figure 4(c), we see that a full revolution of the frame $(\mathbf{h}', \mathbf{v}')$ obliges passage through regions of both signs of trace. Thus there is no path around R on which the trace of the index $+1$ point remains of constant sign, nor on which it is identically zero. Intuitively this shows that there are at least two curves of trace zero connecting the boundaries of R (hence Hopf bifurcation, because the index is $+1$). Appendix A makes this final point of the argument rigorous.

1.5.4. *Neutral saddle curves.* One might hope that the same argument would apply to the index -1 part of E but d_xG reverses orientation there so $(\mathbf{h}', \mathbf{v}')$ is negatively oriented and although it performs a full revolution this does not restrict the sign of the trace. So how may the curves of neutral saddle from the B points join up?

One way is that the neutral saddle curves could connect B points in the same pairs as do the Hopf curves; that would generate two rotational curves of trace-zero. They may be of horizontal homotopy type, as sketched in figure 5(a), and as occurs in our example (section 2.4). With only one equilibrium of index $+1$ and one saddle there are generically no self-intersections of the union of arcs with a centre nor of that for a neutral saddle. A priori, there could be intersections of an arc of centre with an arc of neutral saddle, as illustrated in the bottom of Figure 5(a″), but they do not occur in example (3) (which looks like Figure 5(a′)) and they would lead to added complication when one comes to study the effect on curves of contractible homoclinic connection (Section 1.10). So we choose to eliminate them by

Assumption 3b: There is no coexistence of centre with neutral saddle.

Alternatively, the neutral saddle curves could connect the B points in pairs to make two rotational curves of trace-zero of a homotopy type making one horizontal revolution and some non-zero number of vertical revolutions, as sketched in Figure 5(b). For example, take

$$\begin{aligned} \dot{x} &= \Omega_x - \cos 2\pi y - \varepsilon \cos 2\pi(x+y) \\ \dot{y} &= \Omega_y - \sin 2\pi y - \varepsilon \sin 2\pi(x+y) \end{aligned} \tag{9}$$

with $\varepsilon \in (1/\sqrt{2}, 1)$. For $|\varepsilon| < 1$ there are at most two equilibria and the resonance region is a round annulus just as for example (3). It has $\det = -4\pi^2\varepsilon \sin 2\pi x$ so the saddle-node curves are vertical. It has $\mathrm{tr} = 2\pi\varepsilon\sqrt{2}\sin 2\pi(x+y-\frac{1}{8}) - 2\pi\cos 2\pi y$, so for $\varepsilon \in (1/\sqrt{2}, 1)$ then $\mathrm{tr} = 0$ consists of two closed curves homotopic to $x+y=0$, which make one negative vertical revolution for each horizontal revolution. This scenario, however, forces intersections of arcs of centre with arcs of neutral saddle, as illustrated in Figure 5(b′), which we have ruled out by Assumption 3b.

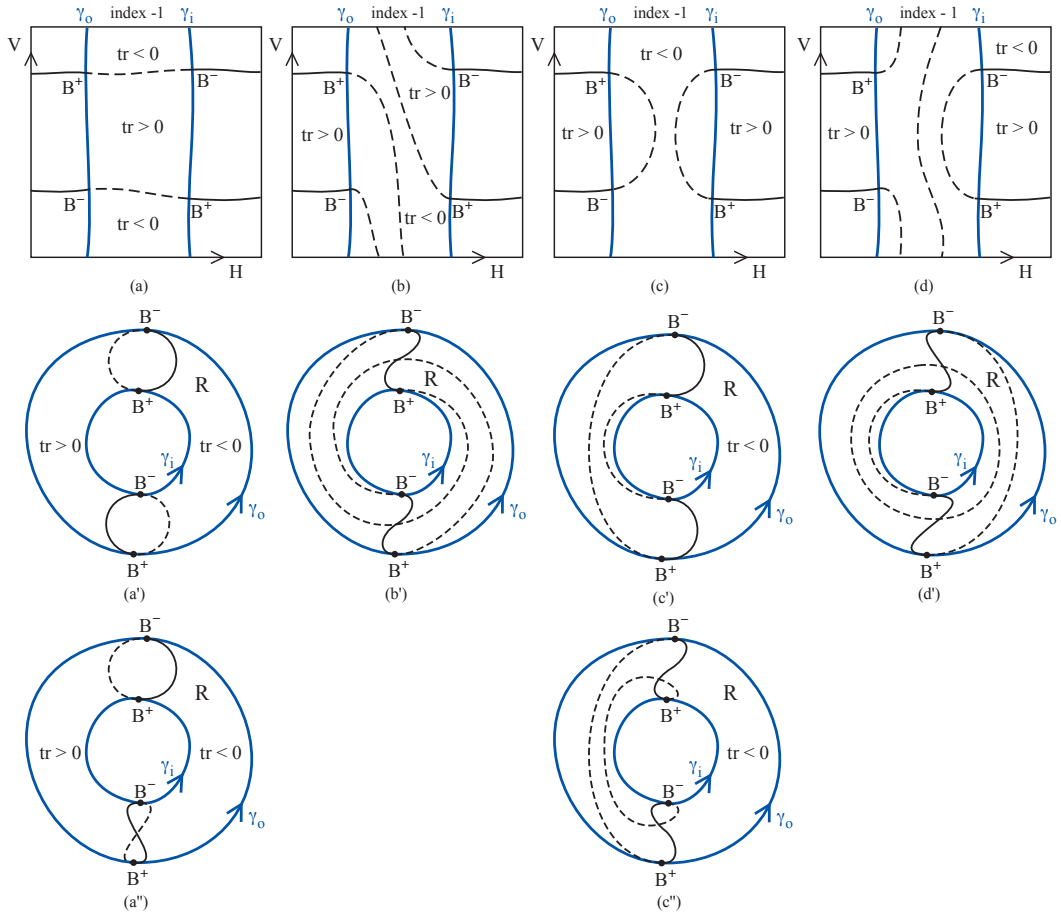

FIGURE 5. Some ways the neutral saddle curves could connect the B points, shown above on the manifold of equilibria and below in projection to parameter space: (a) making two horizontal closed curves of trace-zero – the projections may form simple loops, as in (a′), or may have intersections of neutral saddle with centre as in (a″); (b) making two closed curves of trace-zero which make one horizontal revolution and some non-zero number of vertical revolutions; (c) connecting into a single contractible curve of trace-zero (two ways shown); (d) connecting into a vertical curve of trace zero, necessitating an additional vertical curve of neutral saddle. In some of the projections to parameter space are indicated regions where both equilibria have $\mathrm{tr} < 0$ or $\mathrm{tr} > 0$.

Another way to join up the B points by the neutral saddle curves is to make a single closed curve of trace-zero. It may be contractible or vertical, as sketched in Figure 5(c),(d), respectively. In case (d), there has to be in addition at least one vertical closed curve of neutral saddle to make the sign changes of the trace consistent, but we have declared that to be not simplest (Assumption 3a), so we exclude it. On the other hand, case (c) is permitted by our assumptions so far and is realisable, e.g. add $\eta \sin 4\pi y$

to $\dot{y}$ in (9), take $\varepsilon = \frac{1}{\sqrt{2}}$ and η small positive or negative. Two variants of case (c) are drawn.

One might propose that we should regard case (c) of Figure 5 as simpler than case (a), because it has fewer trace-zero curves, but it has the same number of arcs of Hopf and of neutral saddle, so we prefer to keep both options open, but with no intersections of centre and neutral saddle curves (Assumption 3b), so from case (c) we keep only (c′).

1.5.5. *Additional remarks.* We close this section with a few further remarks.

Firstly, the curves of contractible homoclinic connection coming out of the B points also have to end somewhere. This will be examined in section 1.10.

Secondly, a potentially useful result for the saddles is that their eigenvectors perform half a revolution for a full revolution of parameters around R. This is because there is an eigenvector with positive eigenvalue in the angle less than π between any vector and its image under d_xG. Thus as $\mathbf{v}$ of section 1.5.3 makes no revolutions and $\mathbf{v}'$ makes one revolution, the expanding eigenspace E^u makes half a revolution.

Thirdly, one can also prove existence of non-vertical rotational closed curves $\sigma^{\pm}$ on E on which $\mathbf{v}$ is an eigenvector with positive/negative eigenvalue, respectively. This is because we can lift the vertical foliation of R to the whole of E, and $\mathbf{v}' \neq 0$ (by the argument of section 1.4 on the sne curves and invertibility of d_xG elsewhere) and makes one revolution as the base point of $\mathbf{v}$ and $\mathbf{v}'$ makes one revolution around R. So on each closed curve homotopic to vertical, there is at least one point where $\mathbf{v}'$ is positively parallel to $\mathbf{v}$ and one point where it is negatively parallel to $\mathbf{v}$. By an argument similar to Appendix A (with the role of tr replaced by the sine of the angle from $\mathbf{v}$ to $\mathbf{v}'$), the sets where these happen must contain rotational curves of a non-vertical homotopy type.

Fourthly, the annulus bounded below by σ^- and above by σ^+ contains a curve of centres connecting the B points (already found) and it is surrounded by a zone of foci, bounded by a closed curve of improper node. The centres and foci in this annulus have negative (i.e. clockwise) rotation. In the other annulus, they rotate positively.

1.6. **Flow in the hole.** Extending [BGKM2] to monotone families, for a parameter value $\mathbf{\Omega}$ in the hole, the vector field performs one revolution as $\mathbf{x}$ performs one vertical revolution on the torus. This is because we can write

$$G(\mathbf{\Omega}, \mathbf{x}) = \int_{\mathbf{\Omega}^e(\mathbf{x})}^{\mathbf{\Omega}} d_\Omega G(\tilde{\mathbf{\Omega}}, \mathbf{x})\, d\tilde{\mathbf{\Omega}}, \tag{10}$$

which, taking a straight-line path in $\tilde{\mathbf{\Omega}}$, satisfies $\langle G(\mathbf{\Omega}, \mathbf{x}), (\mathbf{\Omega} - \mathbf{\Omega}^e(\mathbf{x}))\rangle \geq c\, |\mathbf{\Omega} - \mathbf{\Omega}^e(\mathbf{x})|^2$ by monotonicity. For $\mathbf{\Omega}$ in the hole and a vertical closed curve on $\mathbb{T}^2$, then $\mathbf{\Omega} - \mathbf{\Omega}^e(\mathbf{x})$ makes one revolution. Thus so does $G(\mathbf{\Omega}, \mathbf{x})$.

Similarly, as $\mathbf{x}$ follows a horizontal closed curve on the torus, the vector field makes no revolutions. So, following a closed curve of homotopy type (m, n), the vector field makes n revolutions.

This implies that the flow has no cross-section (a *cross-section* for a flow is a transverse section such that the forward and backward trajectories of every point hit it). To see this, a cross-section can not be homotopically trivial because everything that crosses a homotopically trivial transverse section has no opportunity to cross again. There is no transverse section of homotopy class other than horizontal because if there were a

transverse section of type (m, n) with $n \neq 0$ the vector field would make n revolutions for one revolution along the section, contradicting transversality. If there were a horizontal cross-section Σ then one could foliate the torus by horizontal cross-sections Σ_λ given by flowing from Σ for a fraction $\lambda \in [0, 1)$ of the return time. But then the vector field would make no revolutions for one vertical revolution of the base point, contradicting the result of the first paragraph of this section.

A vector field on the torus without equilibria nor cross-section has a periodic orbit [S]. Because Siegel did not state his result in this way, we summarise the proof. Firstly no equilibria implies there is a transverse section T (take any orbit of the perpendicular vector field $G^\perp$ to G, it has a limit point and it is not an equilibrium, the orbit has a close recurrence near there, so close off the recurrence at a shallow angle to make a transverse section to G). The section T is horizontal by the previous paragraph. As there is no cross-section, T is not a cross-section, so at least one semi-orbit never hits it. Taking a $\mathbb{Z}$-cover, such a semi-orbit is trapped in an annulus between copies of the transverse section. Because there are no equilibria, the Poincaré-Bendixson theorem implies its limit set is a periodic orbit.

A periodic orbit for such a flow can not be contractible (else it would surround an index +1 equilibrium). Up to sign, all periodic orbits are of horizontal homotopy type because for homotopy type (m, n) the vector field would have to make n revolutions.

To complete the analysis, we use the decomposition theory of [NOB]. Applied to our case of a vector field on the torus with no equilibria and at least one horizontal periodic orbit, it implies that the flow consists of horizontal periodic orbits and horizontal annuli of two possible types, which we call "ordinary" and "Reeb". Figure 6 shows four versions of each to cater for all possible orientations.

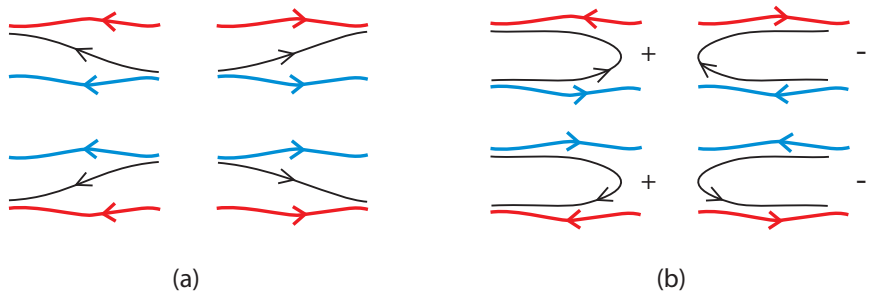

FIGURE 6. (a) Ordinary and (b) Reeb components (indicating the sign of the half-revolution of the vector field from bottom to top) (online colour convention for periodic orbits: red is attracting, blue is repelling).

The vector field in a Reeb component makes $\pm\frac{1}{2}$ revolution from the bottom to the top, whereas in an ordinary component it makes none. By our condition on the rotation of the vector field on making one vertical revolution, we deduce that there are at least two Reeb components of positive half-rotation.

As our example has just two Reeb components (section 2.7), we make:

Assumption 4a: There are at most two Reeb components for flows in the hole.

Supported by our example (section 2.7), and to minimise the number of invariant annuli, we also add:

Assumption 4b: There are no other invariant annuli for flows in the hole.

Then the flow for parameter values in the hole looks like Figure 7, with a repelling periodic orbit travelling rightwards and an attracting one travelling leftwards.

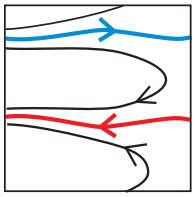

FIGURE 7. The flow for parameter values in the hole, under Assumptions 4a,b.

1.7. **Flow outside the resonance.** For parameter values $\mathbf{\Omega}$ outside the resonance region (meaning in the unbounded component of the complement of R), the vector field makes no revolutions as $\mathbf{x}$ makes any revolution on the torus (use (10) again).

This is not enough to deduce that the vector field has a cross-section. There could be two or more Reeb components with half-rotations adding up to zero. But a Reeb component of positive half-rotation is bounded by an attracting left-going periodic orbit and a repelling right-going one, and a Reeb component of negative half-rotation is bounded by an attracting right-going periodic orbit and a repelling left-going one (see Figure 6(b)). So if there are Reeb components outside the resonance and we exclude the case where they both have saddle-node periodic orbit (snp) boundaries then there are at least four rotational periodic orbits. Generic unfolding of the case of Reeb components with snp boundaries produces at least four too. This makes at least four invariant annuli. In the spirit of minimising the number of invariant annuli, and realisable by our example in section 2.5, we assume

Assumption 4c: There are no Reeb components for parameter values outside the resonance region.

It follows that outside the resonance region, the vector field has a cross-section. We call the flow of a vector field on $\mathbb{T}^2$ with a cross-section (and forcibly no equilibria) *Poincaré flow* [BGKM1]. It has a "homology direction" on the unit circle (direction of the average velocity on the universal cover) such that every trajectory on the universal cover lies within a bounded distance of a straight line of that direction and goes to infinity in that direction, and in the opposite direction for negative time. If the homology direction is rational $(m,n)/\sqrt{m^2+n^2}$ with no common factor between m and n, then there is at least one periodic orbit of homotopy type (m,n), and all periodic orbits have the same homotopy type. Generically, they are alternately linearly attracting and repelling, or in codimension-one they can be generic saddle-node periodic orbits.

A further step in the direction of minimising the number of invariant annuli would be to assume at most two rotational periodic orbits for flows outside R, but it is not clear that we could prove it in our example, even for just horizontal homotopy type. Furthermore, it fails in R, because there is a region with three rotational periodic orbits (see section 1.12).

For irrational homology direction, under our smoothness assumption the flow is topologically conjugate to that of a constant vector field with the given irrational direction (Denjoy's theorem; see [M] for a renormalisation proof). Possession of a given irrational homology direction is a codimension-one property. This can be proved by the formula for the parameter-derivative of rotation number for circle maps in [YM].

Also (10) implies that the vector field at any point makes one revolution as $\mathbf{\Omega}$ makes one revolution. We deduce that the homology direction makes one revolution as $\mathbf{\Omega}$ does. So we obtain at least one strip for each rational homology direction, whose boundaries correspond to saddle-node of periodic orbits, interspersed by curves for irrationals.

1.8. **Z points and curves of rotational homoclinic connection.** In this section we study rotational homoclinic connections of horizontal homotopy type.

1.8.1. *Inner saddle-node curve.* We start by examining bifurcations that may occur along the inner saddle-node curve, following the line of argument of [BGKM2].

The saddle-node performs one vertical revolution as the parameter rotates positively round the inner saddle-node curve (Figure 1(b)). But the repelling and attracting periodic orbits for a closed parameter-loop just inside the inner saddle-node curve do not make any net vertical revolutions as the parameter changes, because the path in parameter space can be contracted to a single parameter value in the hole. Thus the Reeb components make no net vertical revolution as the parameter performs a circuit, so the saddle-node has to rise through the Reeb components. This implies it "crosses" each of the periodic orbits at least once. The way a saddle-node crosses a periodic orbit is to form a rotational homoclinic cycle to the saddle-node (saddle-node loop), which absorbs the periodic orbit into a saddle-node on an invariant circle[2] (snic) and then later to undergo another rotational saddle-node loop bifurcation to regenerate the periodic orbit on the other side. Thus there are at least four Z points (parameter points with a rotational saddle-node loop) on the inner saddle-node curve.

The Z points are of four distinct types. Firstly, those involved with an attracting periodic orbit have an attracting saddle-node (meaning tr < 0), and those involved with a repelling periodic orbit have a repelling saddle-node (tr > 0). In our case, the attracting periodic orbit goes to the left and the repelling one to the right, so we can label the Z points with $\pm$ for right/leftward homoclinic cycles. Secondly, the cycle has an angle less than π towards the side on which it interacts with the periodic orbit, so we can label the Z point with a, b according as the angle faces above or below the cycle. Thus the minimal sequence of bifurcations on travelling anticlockwise around the inner saddle-node curve is $Z_a^-, Z_b^-, Z_a^+, Z_b^+$.

As our example has precisely four Z points on the inner saddle-node curve (section 2.7), we make:

[2]Some authors call it a central homoclinic to a saddle-node.

Assumption 5a: There are at most four Z points on the inner saddle-node curve.

See Figure 8 for the unfolding of a Z point.

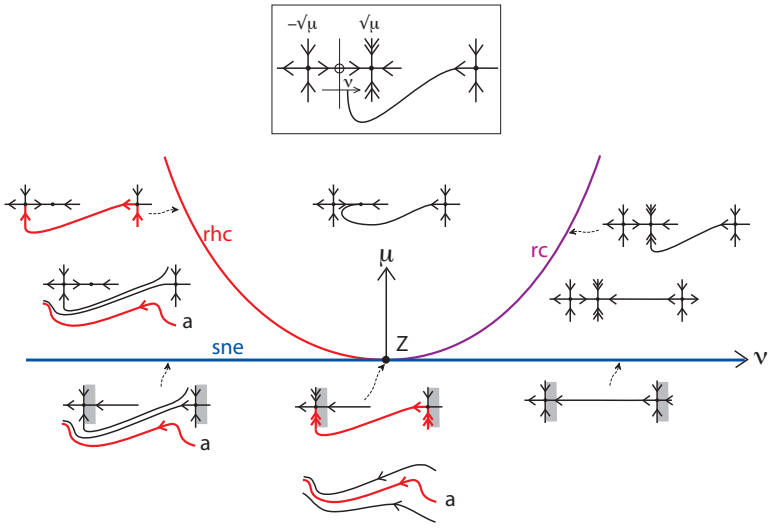

FIGURE 8. The unfolding of a Z point (case Z_b^-). The diagram at the top indicates the unfolding parameters (μ, ν). The curve rc is a curve of rapid connection, meaning that the unstable manifold of the saddle goes into the fast direction at the node (adapted from [BM1]).

A question is where the B points lie relative to the Z points. If the parameter value crosses the saddle-node curve from the hole at a B point, generically the B point is born in one of the Reeb components because it would be a codimension-three phenomenon to have its invariant manifolds form a cycle. Thus for the flow at B^- we have two apparent possibilities, according to the Reeb component containing the sne (Figure 9(a),(b)).

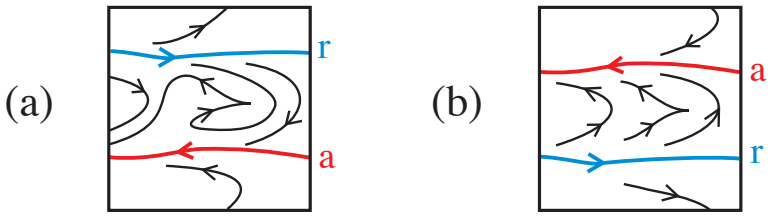

FIGURE 9. The two apparent possibilities for the flow at the inner B^- point. We rule out case (a).

As we turn anticlockwise from the B^- point, the saddle-node becomes attracting (meaning it has tr < 0). So possibility (a) would require the saddle-node to remain below the repelling periodic orbit all the way until past the B^+ point when it becomes repelling; then it could rise through the repelling periodic orbit with a Z_a^+ followed by

Z_b^+, but would find itself stuck below the attracting periodic orbit until past B^-. This would contradict its starting position.

Thus the phase portrait at the inner B^- point must be possibility (b). Similarly we obtain its analogue for the inner B^+ point. As a consequence, the sequence of bifurcations is $B^-, Z_a^-, Z_b^-, B^+, Z_a^+, Z_b^+$ in anticlockwise order, as shown in figure 10.

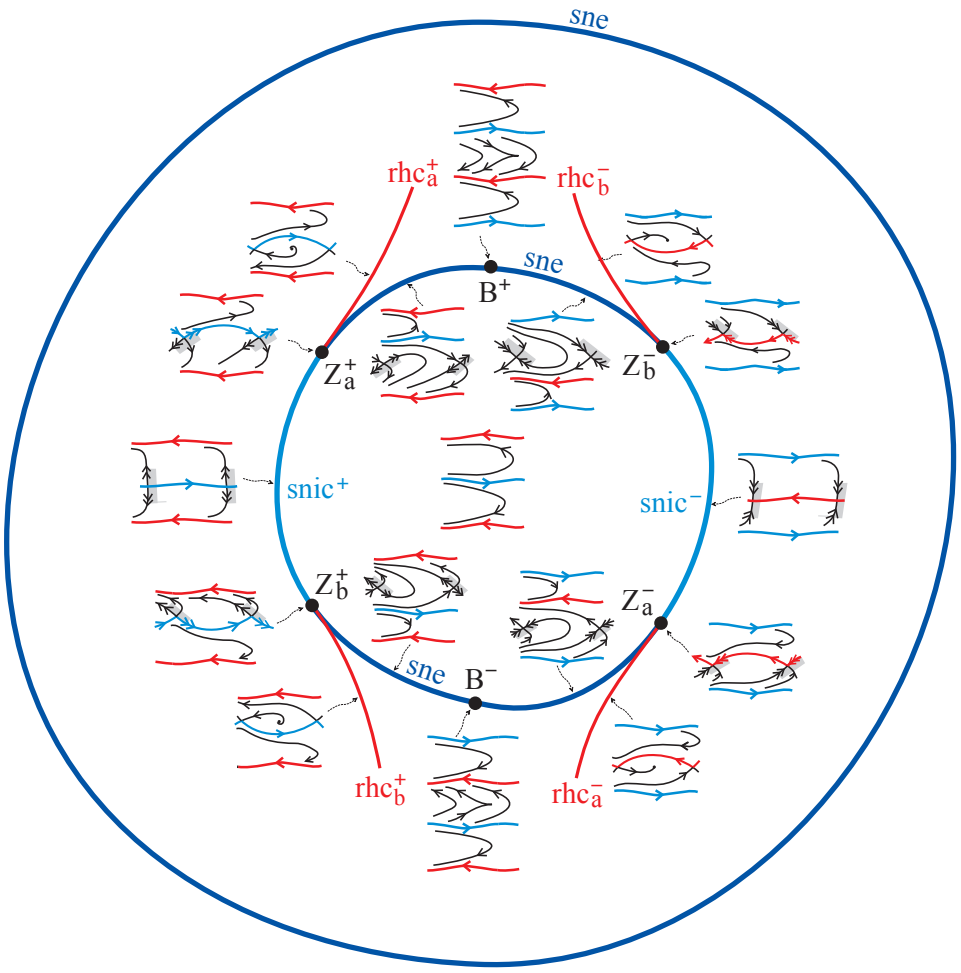

FIGURE 10. The order of bifurcations around the inner saddle-node curve of the resonance region. An extra copy of a Reeb component is shown for each of the B points to facilitate seeing how the saddle-node rises through the Reeb components on turning anticlockwise round the inner saddle-node curve. (The online colour convention is extended to homoclinic orbits: red for attracting, blue for repelling.)

Note that from a Z point comes a curve of rotational homoclinic connection (rhc) to a saddle. It leaves the Z point tangent to the saddle-node curve in the direction of creation of the periodic orbit. Here the periodic orbits are those left over from the Reeb

components in the hole, so the direction of the rhc curves is as shown in figure 10, where they are labelled analogously to the Z points.

1.8.2. *Region of attracting cycle.* The arc of the inner saddle-node curve between Z_a^- and Z_b^- is an arc of snic$^-$ (i.e. saddle-node on invariant circle going leftwards). On crossing the saddle-node curve it produces a C^1 attracting invariant circle containing the saddle and node. How can this attracting invariant circle be destroyed as parameters vary?

To cater for the possibilities that the saddle manifolds pass through a "rapid connection" (meaning that one of them enters the attracting node along its faster eigenvector, as in Figure 8), and afterwards come into the node from the same side, or the node becomes a focus, or even further undergoes Hopf bifurcation, we enlarge the scope from C^1 attracting invariant circle to consider attracting invariant sets of the homotopy type of a horizontal circle, containing the saddle and index +1 point, which we call "attracting cycles".

The parameter-region AC of attracting cycle can not include the outer B points because generically a B point is not on a cycle (that is a codimension-three event, as already mentioned); so there is no attracting cycle in a parameter-neighbourhood. Thus the connected component of the region of attracting cycle connected to the arc of inner snic$^-$ can not extend as far as the outer B points.

In the absence of further equilibria, destruction of an attracting cycle requires an rhc or a snic (with tr < 0 in both cases). Indeed it was created by a snic$^-$, and near the Z points the curves of $\mathrm{rhc}^-_{a,b}$ from the inner $Z^-_{a,b}$ destroy it, generating leftward periodic orbits in its place. We will now prove that the parameter-region AC of attracting cycle connected to the arc of inner snic$^-$ must reach the tr < 0 part of the outer saddle-node curve. It is destroyed there in a snic$^+$, generating an attracting rightward periodic orbit.

Firstly, by our Assumption 5a it is not possible for the curves of $\mathrm{rhc}^-_{a,b}$ to return to the inner sne curve. Secondly, they can not close off the connected component of AC by intersecting because one can not have simultaneous left-going homoclinic connections above and below (there is only one saddle). The boundary of AC can not contain $\mathrm{rhc}^-_{a,b}$ up to the outer sne because the saddle and index 1 point move in opposite directions from the inner to the outer boundary, making a horizontal loop on the torus, but the index 1 point can not cross the stable manifold of the saddle to make the tr < 0 outer saddle-node. The boundary of AC can transition from rhc^-_a to rhc^+_b, however, via what we christened a "necklace" point N in [BGKM1]. Similarly, it can transition from rhc^-_b to rhc^+_a via a necklace point. To prevent AC connecting to the outer B points (as required above), we must have these transitions. Furthermore, the $\mathrm{rhc}^+_{a,b}$ must extend to the tr < 0 part of the outer sne, because they can not intersect each other nor any of the other rhc curves except $\mathrm{rhc}^-_{b,a}$ respectively, but eventually the boundary must end with intersections of $\mathrm{rhc}^+_{a,b}$ and the outer sne.

Thus we have proved that anticlockwise from B^+ to B^- on the outer sne curve we pass through first a Z_b^+ point and then a Z_a^+ point, bounding an arc of snic$^+$; see figure 11.

Considering the region of repelling cycle, the analogous sequence happens on the tr > 0 side. So we have shown that there are at least four Z points of horizontal homotopy types on the outer boundary, in the anticlockwise order $B^+, Z_b^+, Z_a^+, B^-, Z_b^-, Z_a^-$.

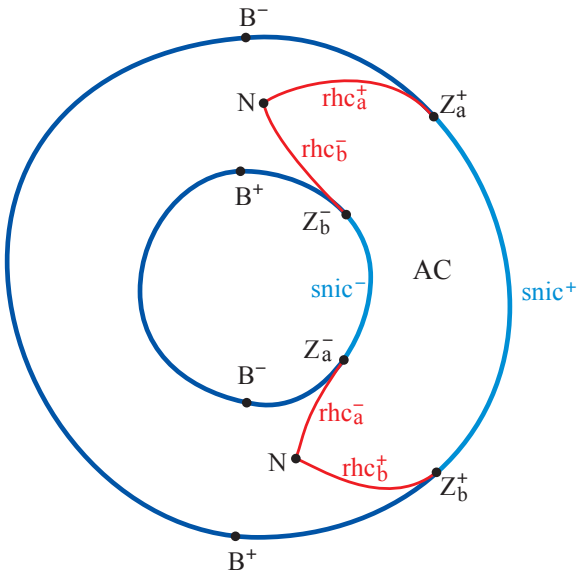

FIGURE 11. The connected component of the region AC of attracting cycle (invariant set of homotopy type of a horizontal circle, containing the saddle and index +1 equilibrium) which has the inner arc of snic$^-$ in its boundary.

Our example has four Z points of horizontal homotopy types on the outer sne (section 2.7). Thus we make:

Assumption 5b: There are no more than four Z points of horizontal homotopy types on the outer saddle-node curve.

The eight Z points of horizontal homotopy type (four inner and four outer) create eight semi-arcs of rhc of horizontal homotopy type. If they join in pairs, they make four curves of rhc (one of each type rhc$^{\pm}_{a,b}$). To minimise the number of rhc curves of horizontal homotopy type we make:

Assumption 5c: There are no more than four curves of rhc of horizontal homotopy types,

as is satisfied by our example (section 2.7). In particular, this rules out closed curves of rhc of horizontal homotopy type, and arcs of horizontal rhc arising from other sources such as pendant points [BGKM1] (which will be reviewed in section 1.10).

1.9. **Necklace points.** Now we consider how the pictures for the regions of attracting and repelling cycle connect.

The points of transition in the boundary of AC from one type of rhc to another are necklace points (parameter points with rhc in opposite directions from the same saddle). It is natural to minimise their number. Our example has just two (section 2.8.2), so we make:

Assumption 6: There are at most two necklace points.

This forces the curves of rhc to be arranged as in Figure 12.

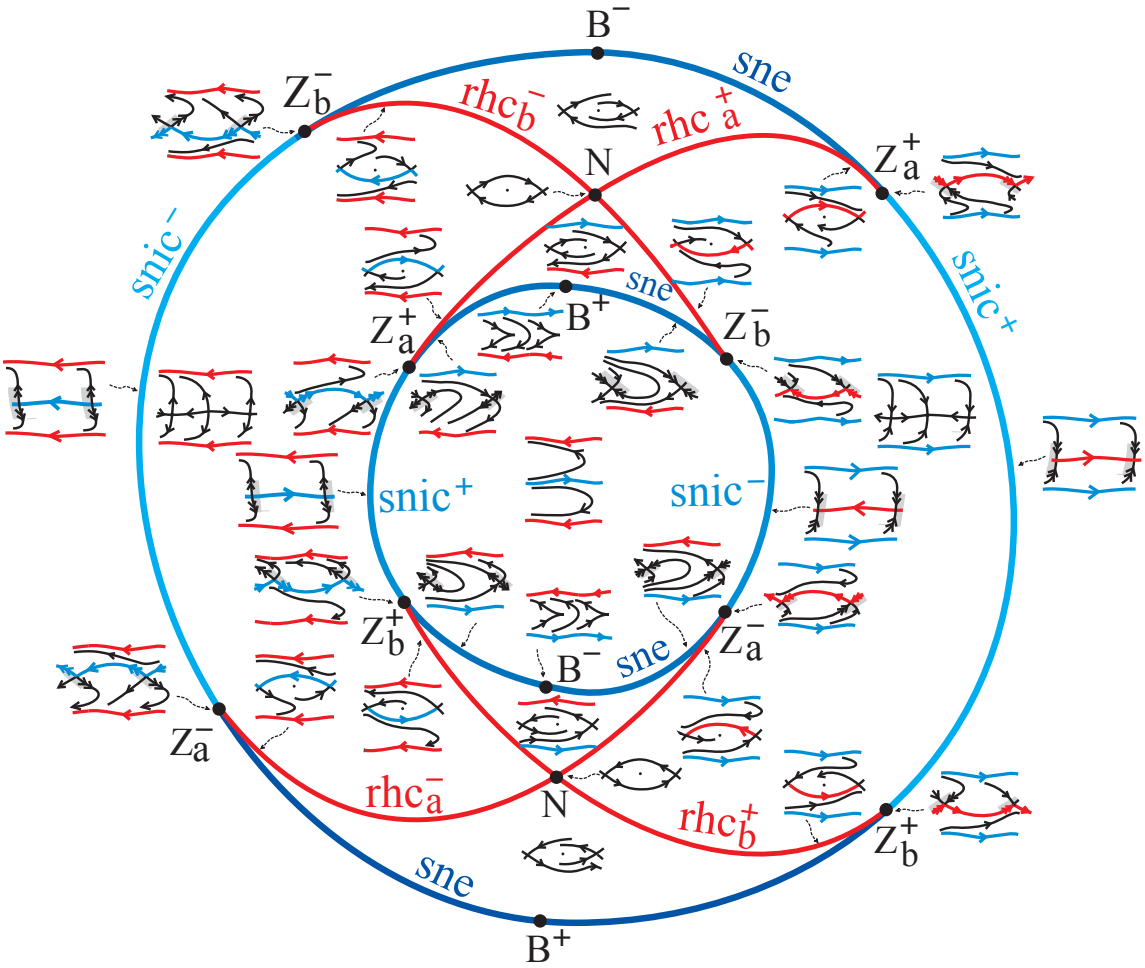

FIGURE 12. The minimal arrangement of curves of horizontal rhc.

In addition to being a crossing of two curves of rhc in opposite directions, which each generate rotational periodic orbits on one side, a necklace point generates two curves of contractible homoclinic connection (chc) [BGKM1]. See Figure 13. Necklace points are an example of gluing bifurcation [GGT].

In the context of figure 12, the curves of chc occur in the sectors above and below the N points. Specialising to the top N point, the chc curves come out tangent to the rhcs to the left/right according as the saddle has tr positive/negative there. The curves of chc produce a contractible periodic orbit (cpo) in the sector of parameter space between them. Under some more assumptions, this will lead to Figure 15.

Before deriving the global picture for the curves of chc, we remark that when there are at most two equilibria an N point on the torus must coexist with a rotational periodic

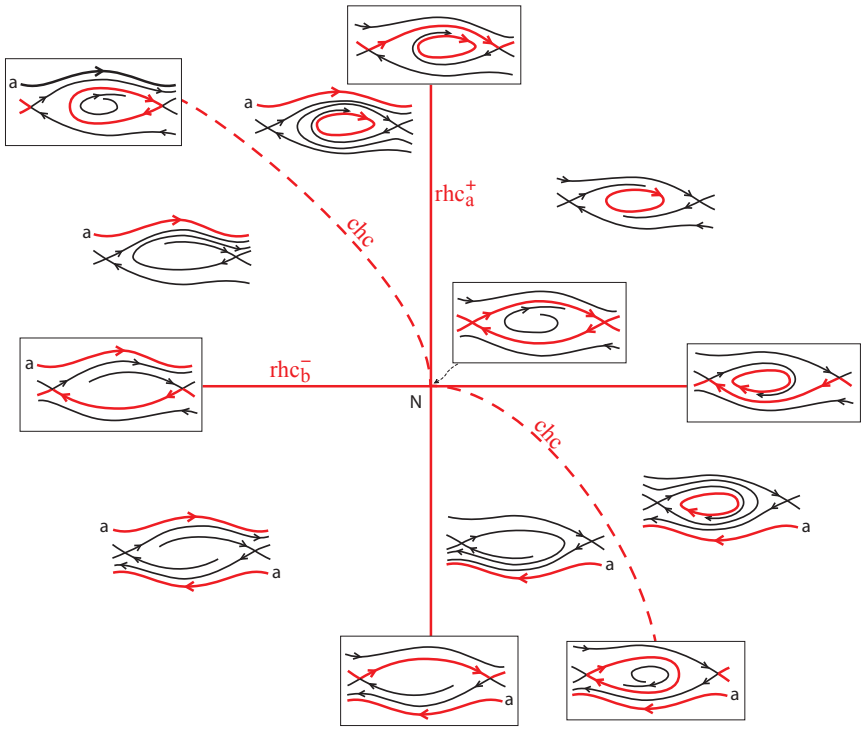

FIGURE 13. Unfolding of a necklace point (drawn for the case of tr < 0 at the saddle) (based on [BGKM1]).

orbit, which is attracting/repelling according as the saddle has positive/negative trace, because the necklace is repelling/attracting and surrounds the index $+1$ equilibrium.

1.10. **Curves of contractible homoclinic connection.** We have seen that each B point produces an arc of chc and each N point produces two arcs of chc. In this section we address the question of how they join up.

If a curve of chc crosses a curve of horizontal rhc then, because it is the same saddle for both, it makes a "pendant" point P [BGKM1]. Pendant points are another type of gluing bifurcation, with one contractible and one rotational homoclinic orbit (see Figure 14 for its unfolding). A pendant generates two additional arcs of rhc (tangent to the original rhc). This would increase the number of curves of horizontal rhc, so under Assumption 5c it does not occur.

Thus we deduce that the curves of chc stay in the sectors bounded by the horizontal rhc curves and so join the N point to the corresponding B points.

Next we ask what happens if a curve of chc crosses a curve of ns. An intersection generically makes what we call a J point [BGKM1]. It generates an arc of contractible snp and a tongue with two cpos, which adds complication. Our example (3) has no J points (section 2.8.3), so we make

Assumption 7a: There are no contractible homoclinic connections to a neutral saddle (J points).

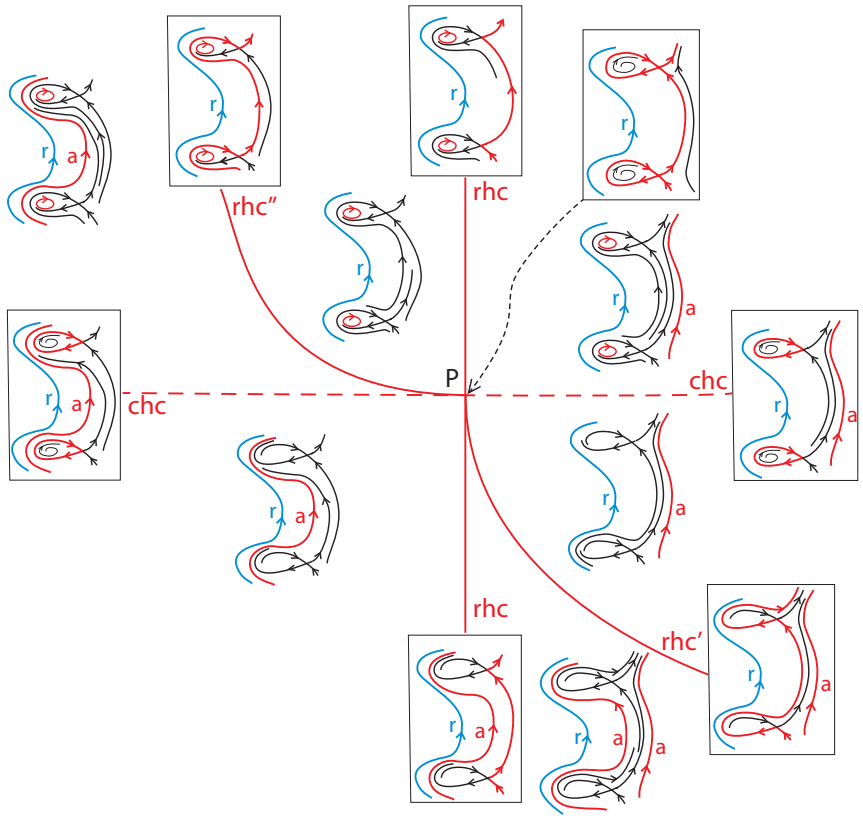

FIGURE 14. Unfolding of a pendant point (case of tr < 0 saddle). The rhc has been chosen non-horizontal and a coexisting repelling periodic orbit added, to correspond to the discussion about the tongue of type (p', q') in Figure 21 (based on [BGKM1]).

Lastly we ask what happens if a curve of chc crosses a curve of centre. This implies that in one sector the centre creates a small cpo and the chc creates a large cpo, making two cpos. Unfortunately, this is what happens in example (3) (section 2.8.3), but we believe there are examples with at most one cpo. Thus we strengthen Assumption 7a to:

Assumption 7b: There is at most one contractible periodic orbit.

We deduce that the curves of chc are arranged as in Figure 15.

To conclude this section, we remark that intersection of a curve of centre with one of ns obliges a curve of chc to produce one of the above scenarios, which is why we chose to rule it out already by Assumption 3b.

1.11. **K points.** Next, we consider the curves of neutral saddle from the B points. Whatever option they choose from subsection 1.5.4, they must intersect the curves of horizontal rhc because the latter connect the inner and outer sne boundaries. We call

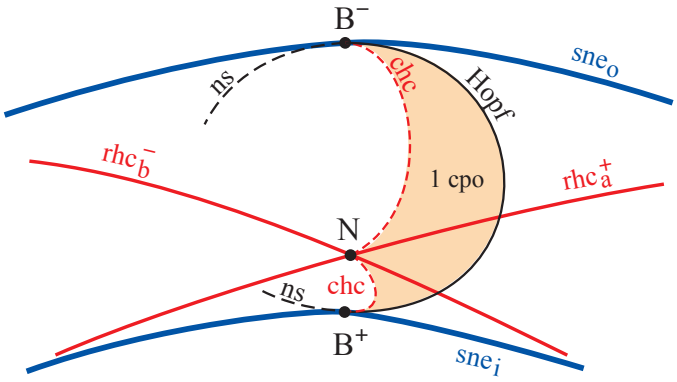

FIGURE 15. Bifurcation diagram for the top of the resonance, showing the region of one contractible periodic orbit between arcs of chc and Hopf bifurcation. The arcs of neutral saddle may join up here or go to the B points at the bottom, as in Figures 5(a′,c′).

such an intersection a K point [BGKM1]. See Figure 16 for the unfolding of a K point. It generates a curve of snp of horizontal periodic orbit, left- or right-going as for the rhc. The curve of snp comes out tangent to the curve of rhc.

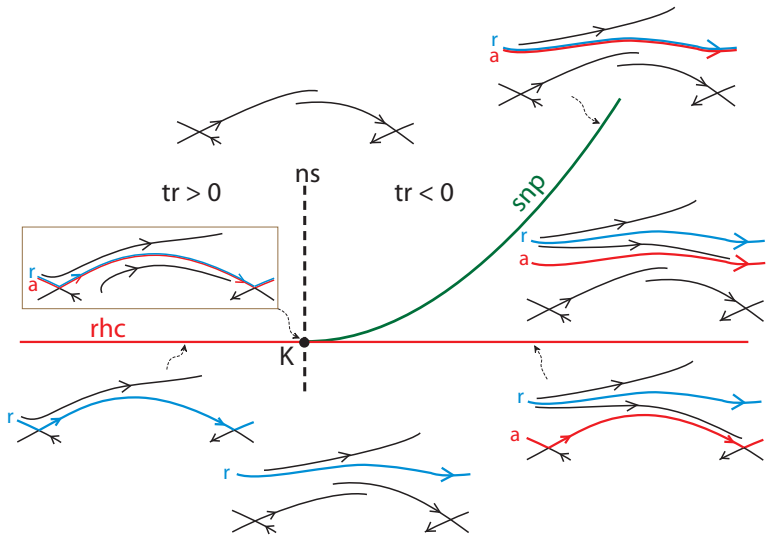

FIGURE 16. The unfolding of a K point (adapted from [BM1]).

In our example, there are precisely two K points on each arc of neutral saddle (section 2.8.5) so we make:

Assumption 8: There are at most four K points for horizontal homotopy type.

To determine the directions in which the K points generate arcs of snp requires study of the directions in which the rhc is broken and the trace changes sign. In the case of

just two K points in the top of the resonance, they come out as shown in Figure 17. The orientation of parameter space in Figure 16 fits the lower K point of Figure 17.

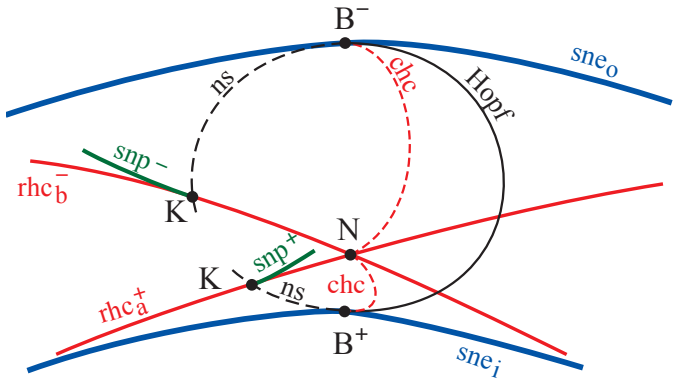

FIGURE 17. Existence of K points and the beginnings of the resulting arcs of snp.

1.12. **H points.** To complete the global bifurcation diagram around the top of the resonance, we know from section 1.7 that there are curves of $\mathrm{snp}^{\pm}$ outside R and that the sector above the necklace point has an attracting and repelling pair of right-going periodic orbits. So the curves of snp from the K points must connect to those outside. There could be additional complications, like swallowtails in the snp curve or additional isola of snp. We could eliminate the former by assuming there are at most two rotational periodic orbits of each homology direction $(\pm 1, 0)$, but this may be difficult to check in any example.

In any case, there must be an intersection of a curve of snp^{+} with a curve of rhc_b^{-}. The simplest case, one intersection, is shown in Figure 18. This creates what we christened

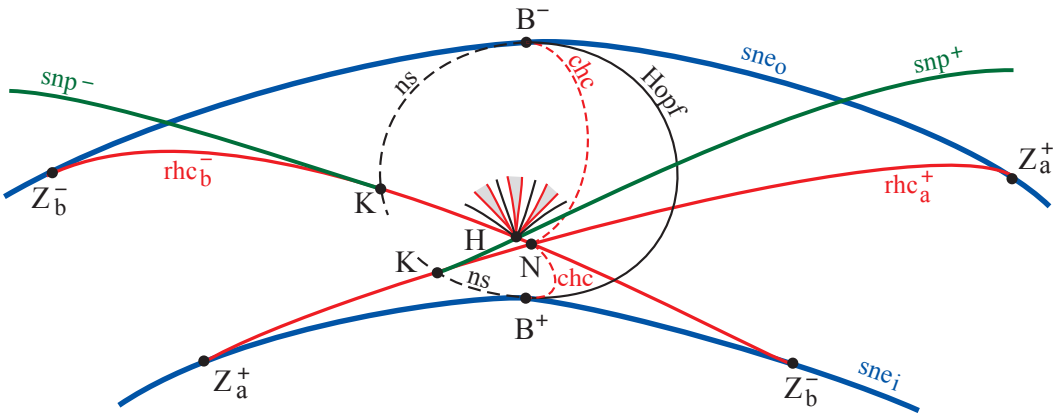

FIGURE 18. Curves of snp, creating an H point.

a (type 2) "half-plane fan" point in [BGKM1], because generically it generates a fan of partial mode-locking tongues with all rational homology directions in a half-plane

between $(\pm 1, 0)$ and intervening curves of irrational homology direction. We call them H points.

We suppose the simplest case:

Assumption 9: There are at most two H points,

which is satisfied by our example (section 2.8.5).

In Figure 19 we have added phase portraits to Figure 18, except for resolving how the trajectories join up vertically in the half-plane fan sector. Note that the bifurcation diagram obliges existence of a triangle KHN in which there coexist three horizontal periodic orbits (two in one direction, one in the other).

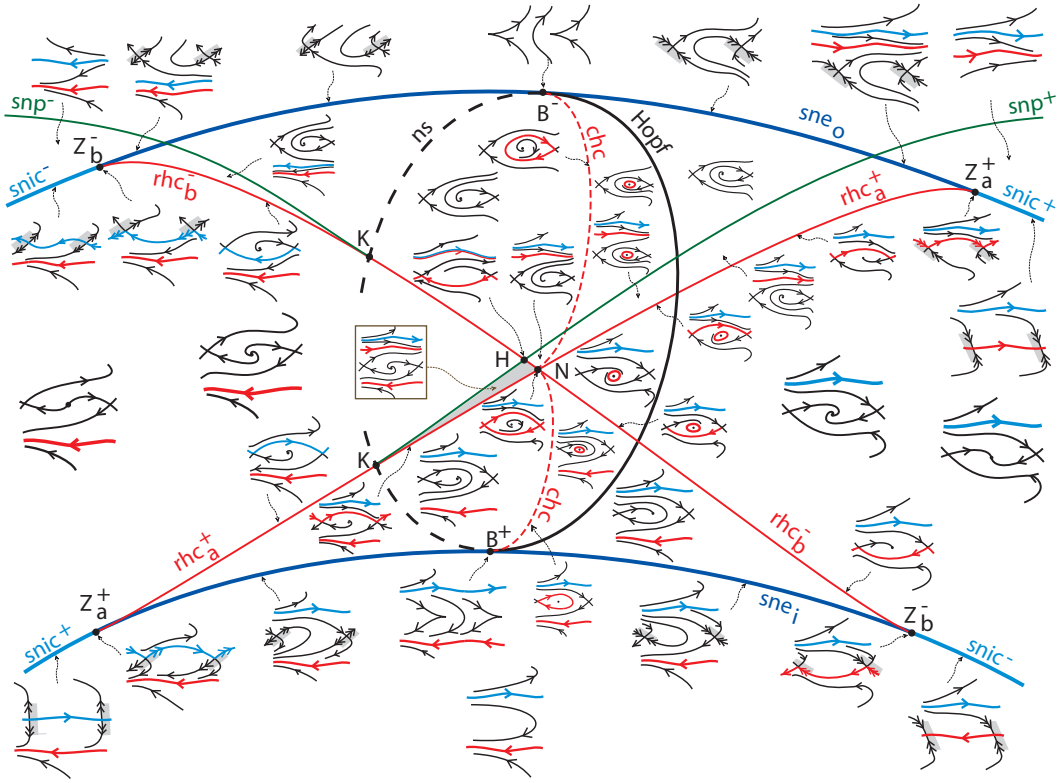

FIGURE 19. Figure 18 with phase portraits.

Figure 20 shows the unfolding of an H point. There are infinitely many ways to insert this into Figure 19, depending on where the B points land in the half-plane fans (alternatively, a B point could be in a partial mode-locking strip of horizontal homotopy type). Generically, the B points land in the interior of a partial mode-locking tongue or strip because to be on a boundary or on an irrational curve is a codimension-3 event.

Each partial mode-locking tongue begins from H with rhc boundaries and a unique rotational periodic orbit [BGKM1], which is attracting or repelling according as tr is negative or positive at the saddle at H. The lefthand rhc goes from the upper right

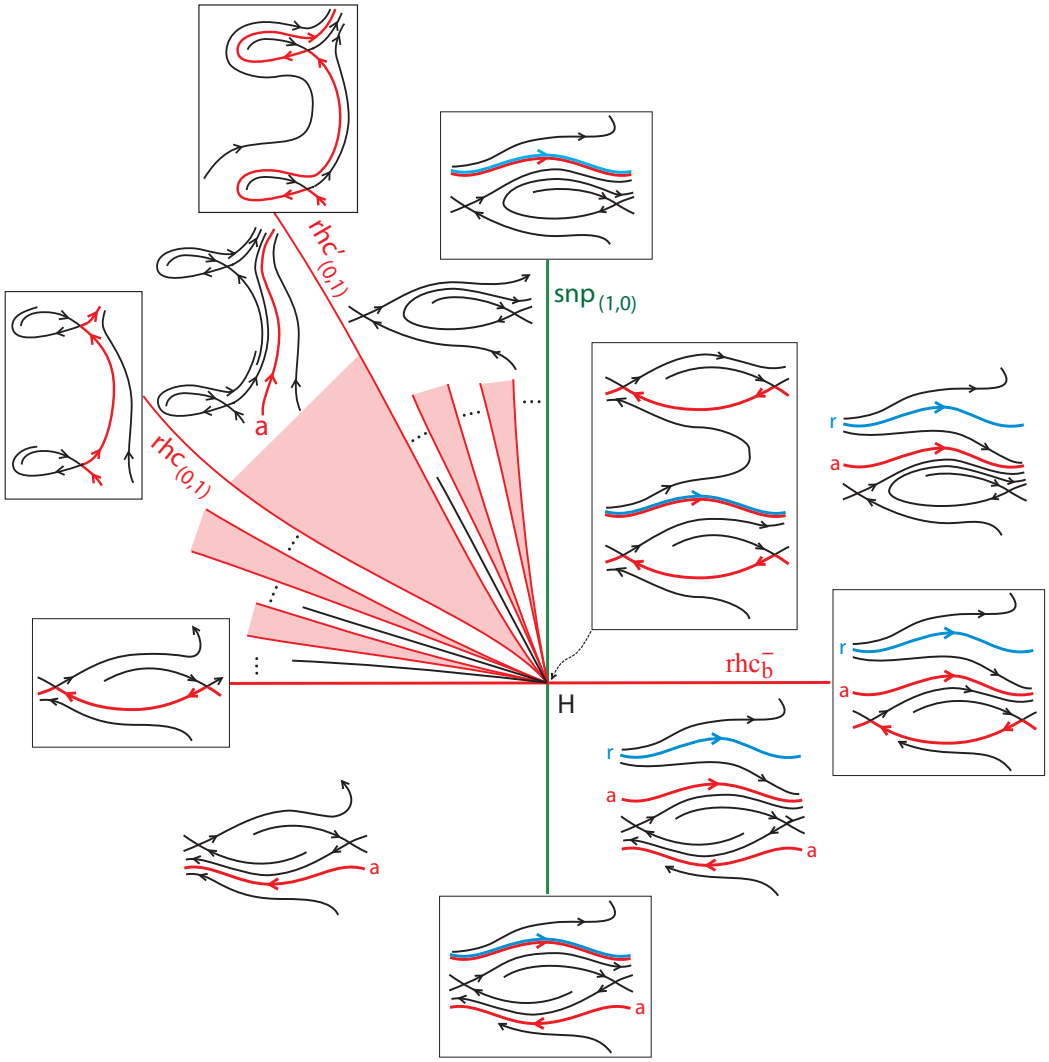

FIGURE 20. The unfolding of a type-2 half-plane fan point (based on [BGKM1]).

branch of unstable manifold of the saddle to the lower right branch of stable manifold of a translate of the saddle. The righthand rhc, which we denote by rhc′, goes from the lower left branch of the unstable manifold of the saddle round the loop and then into the lower right branch of stable manifold of the same translate of the saddle. See Figure 20.

If the rhc crosses the curve of ns, it makes a K point there, generating a curve of snp forming the left boundary of the tongue thereafter. The rhc′ has to cross the curve of ns also, making another K point and generating a curve of snp forming the right boundary of the tongue thereafter. The curves of rhc and rhc′ terminate in Z points on the outer sne. This is sketched as type (p, q) in Figure 21.

If instead, the curve of rhc crosses the curve of chc, it makes a P point there. As was recalled in section 1.10, the P point produces two additional arcs of rhc. One is the end

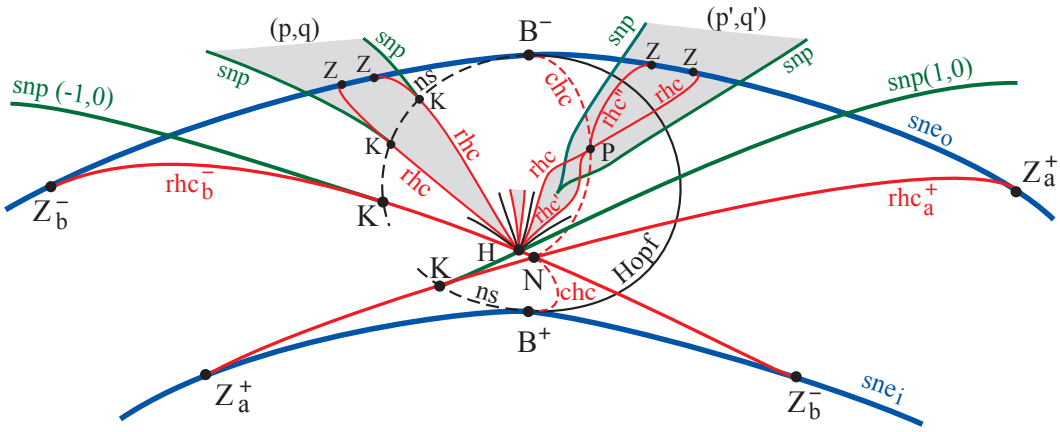

FIGURE 21. The boundaries of all partial mode-locking types in a half-plane fan (type 2) begin as curves of rhc. The partial mode-locking tongues on the left like (p, q) cross a curve of neutral saddle, where the boundary of the tongue converts from rhc to snp by K points. The tongues on the right like (p', q') cross a curve of contractible homoclinic connection in a pendant point: the boundary switches to curves of saddle-node periodic orbit before this.

of rhc$'$, tangent to rhc. The other, denoted rhc$''$, comes out tangent to the curve of chc. The P point also produces contractible and rotational periodic orbits as was shown in Figure 14 for the case of attracting saddle. There is an attracting rotational periodic orbit in all sectors of Figure 14 except between rhc going upwards in parameter space and rhc$''$ (and there are two in the sector between rhc going downwards and rhc$'$), so we deduce that there must be an additional repelling rotational periodic orbit not related to the local bifurcation analysis around P, which saddle-nodes with an attracting one created by the P point further away in parameter space, yielding a curve of snp, which becomes the boundary of the tongue when outside the region bounded by rhcs. The snp curve has to have a cusp because the directions of coalescence of attracting and repelling periodic orbit are opposite on the two snp curves outside the resonance (in [BGKM1] we missed the requirement for a cusp). The result for such a partial mode-locking tongue is sketched as type (p', q') in Figure 21.

As argued earlier in this section, generically there is one partial mode-locking tongue, say of type (p'', q''), with the outer B^- point in its interior. If the unstable branch from the B^- equilibrium passes to the right of the stable branch of the (p'', q'') translate then one obtains a slight deformation of the diagram for (p, q), in which the righthand snp crosses the ns and chc to pass to the right of the B^- point. If instead the unstable branch from the B^- equilibrium passes to the left of the stable branch of the (p'', q'') translate then one obtains the diagram as for (p', q') but with the B^- point in between the lefthand snp and the lefthand Z point.

If we had allowed Reeb components for parameter values outside the resonance region (section 1.7) then another type of half-plane fan point would have been relevant (type 1 in

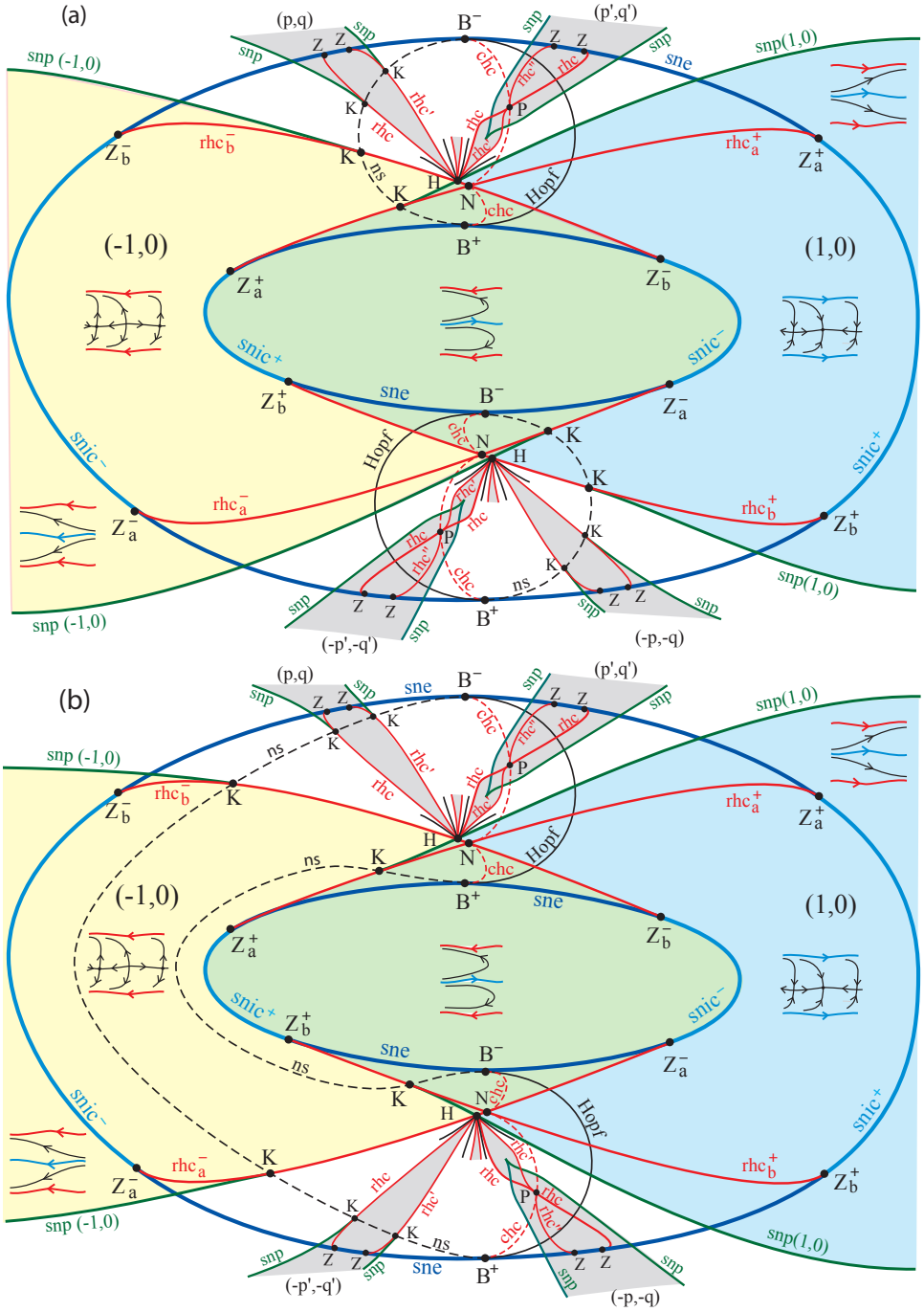

FIGURE 22. (colour online) Representatives of the two simplest bifurcation diagrams for monotone families of vector fields on a torus. The top case (a) has three variants in which the arcs of centre and neutral saddle face other ways. The bottom case (b) has one variant in which they both face the opposite way.

[BGKM1]). It might be worth relaxing Assumption 4c to at most two Reeb components, to allow this case.

1.13. **Conclusion of Part 1 and Outlook.** Putting all our analysis together, under Assumptions 1-9, we have proved that the bifurcation diagrams for monotone families of vector fields on a torus are as in Figure 22. The two cases differ only in the way the neutral saddle curves connect. The upper diagram is that proposed in [BGKM1]. The diagrams for general monotone families of vector fields on a torus must be at least as complicated as these.

To prove that they are the simplest possibilities, in principle we need an existence proof of a family satisfying all the assumptions. In Part 2 we prove that example (3) satisfies all but one (7b) of the Assumptions here. Thus we almost have an existence proof of one of the proposed simplest diagrams. It would be good to make examples satisfying all the assumptions and realising each of the diagrams of Figure 22.

As the next simplest case, one could allow up to two Reeb components for flows outside R; then one would obtain bifurcation diagrams that are not much more complicated, with type-1 half-plane fan points [BGKM1] instead of type-2.

One could study the region of existence of C^1 invariant circles, as in [BM1]; this would require finding curves of rapid connection, as from Z points, which involves the curves of improper node.

It would be nice if one could prove monotonicity of the homology direction with respect to rotation of parameter around the outside of the resonance, in the sense that the set with given homology direction is connected.

Related work for two other types of family of 2D vector fields is reported in [BM1, BM2]. It would be interesting to extend our study to other surfaces, in particular of genus g larger than 1, where the parameter space should have dimension $2g$ to correspond to the first homology group H_1.

2. Example

In this part we show that example (3) satisfies all the Assumptions 1–9 except for 7b, and derive much of its bifurcation diagram.

2.1. **General conditions.** Before starting on checking the above Assumptions, there are three general conditions that we required in the Introduction.

Our first condition is that the family be C^3 in $(\mathbf{\Omega}, \mathbf{x})$, which holds for our example.

Our second condition is that it be monotone with respect to parameters. Our example is monotone with respect to the standard inner product $\langle (x_1, y_1), (x_2, y_2) \rangle = x_1 x_2 + y_1 y_2$.

Our third condition is that all bifurcations have co-dimension at most two and the family be transverse to them. We have checked this property for the principal bifurcations of (3) and we will report on them in the appropriate sections to follow. It is probably unfeasible to check for all because there are infinitely many partial mode-locking types, so instead we appeal to C^3-genericity to deduce that there are arbitrarily small perturbations of our example in C^3 which satisfy this condition.

2.2. **Equilibria.** The equilibria of (3) are given by the equations

$$\begin{aligned} \Omega_x &= \cos 2\pi y + \varepsilon \cos 2\pi x \\ \Omega_y &= \sin 2\pi y + \varepsilon \sin 2\pi x. \end{aligned} \tag{11}$$

The set E of equilibria $(\mathbf{\Omega}, \mathbf{x})$ as a subset of $\mathbb{R}^2 \times \mathbb{T}^2$ is a graph over $\mathbb{T}^2$; denote it by the function $\mathbf{\Omega} = \mathbf{\Omega}^e(\mathbf{x})$ (which is just (11)). Furthermore on E, $\mathbf{\Omega}$ performs epicycles of radii ε and 1 respectively, as x and y rotate around the torus. We assume that $\varepsilon \in (0,1)$, so the set of parameter values with an equilibrium, which we call the "resonance region" R, is $1-\varepsilon \le |\mathbf{\Omega}| \le 1+\varepsilon$, a round annulus, as shown in Figure 23(a). There are precisely two equilibria for each interior point of R and one for each boundary point of R.

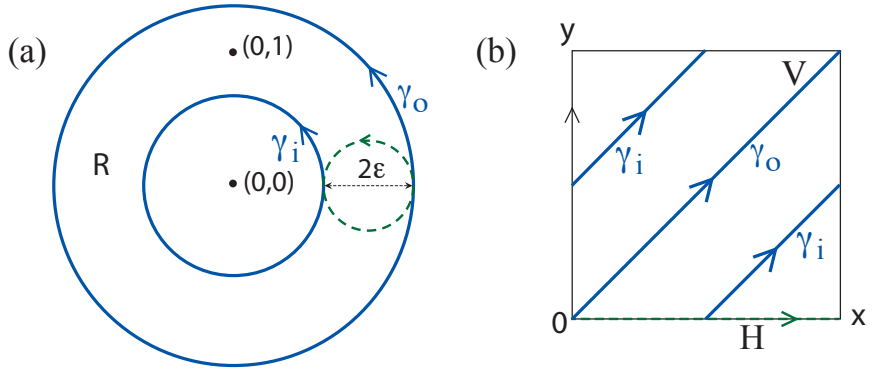

FIGURE 23. (a) The resonance region R for (3); (b) the sne curves γ_i, γ_o in the set E of equilibria, representing homology class V, and a representative of homology class H (dashed line).

Thus Assumption 1 is satisfied.

2.3. **Principal homotopy classes.** We can view E as two copies of R with their inner boundaries glued together and their outer boundaries glued together. The boundaries of R are the images of the fold curves for the mapping from E to the parameter plane $\mathbb{R}^2$.

The boundaries of R correspond to x parallel or antiparallel to y, i.e. $x = y$ (outer boundary) or $x = y + \frac{1}{2}$ (inner boundary). Taking the closed paths $x = y$ and $x = y + \frac{1}{2}$ on $\mathbb{T}^2$ in the direction of increasing x and y produces the boundaries of R taken positively (anticlockwise). Thus homology type $(1,1)$ on $\mathbb{T}^2$ corresponds to the "long" way around E, i.e. projecting to one positive revolution in R without making any net crossings of the fold curves.

Taking the closed path $y = 0$ on $\mathbb{T}^2$ produces a curve $\Omega_x = 1+\varepsilon \cos 2\pi x, \Omega_y = \varepsilon \sin 2\pi x$ on E which performs a loop the "short" way around E, i.e. non-contractible but making no revolutions around the hole in the projection to R. So homology type $(1,0)$ goes the short way around E.

Thus the homology classes V and H of section 1.2 are $(1,1)$ and $(1,0)$ respectively, as shown in Figure 23(b). In section 1.2 we applied a coordinate and parameter change to make $V = (0,1)$ and $H = (1,0)$. We could do that to our example, but it makes the formulae longer, so it is easier just to remember that for our example "vertical"

means $(1,1)$ not $(0,1)$. In this part the vertical is not needed; what is important is the horizontal, which is why we interchanged x and y relative to [BGKM1, BGKM2].

2.4. **Linearisation at equilibria.** Let us linearise the vector field around the equilibria, for tangent orbit $(\delta x, \delta y)$.

$$\begin{bmatrix} \dot{\delta x} \\ \dot{\delta y} \end{bmatrix} = \begin{bmatrix} 2\pi\varepsilon \sin 2\pi x & 2\pi \sin 2\pi y \\ -2\pi\varepsilon \cos 2\pi x & -2\pi \cos 2\pi y \end{bmatrix} \begin{bmatrix} \delta x \\ \delta y \end{bmatrix}. \tag{12}$$

The matrix has determinant

$$\det = 4\pi^2 \varepsilon \sin 2\pi(y-x),$$

so the equilibrium has Poincaré index $+1$ for $0 < y-x < \frac{1}{2}$, -1 for $\frac{1}{2} < y-x < 1$, as shown in Figure 24(a). These two cases correspond to the interiors of the two copies of R that make up E when glued along their boundaries. The determinant is zero precisely on the fold curves, corresponding to degenerate equilibria. For $\varepsilon \neq 0$ they are generic saddle-nodes because the folds are generic; for example at $y = x = 0$ then $\partial_x^2 \Omega_x^e = -4\pi^2\varepsilon \neq 0$, and the rest follow by rotational symmetry of the equilibrium problem.

The linearised vector field has trace

$$\mathrm{tr} = -2\pi \cos 2\pi y + 2\pi\varepsilon \sin 2\pi x. \tag{13}$$

Thus the trace is zero where $\cos 2\pi y = \varepsilon \sin 2\pi x$, which forms two closed curves on E, one near $y = \frac{1}{4}$, the other near $y = \frac{3}{4}$, as shown in Figure 24(a). They have homology type $(1,0)$ as x increases, and project to closed curves in R within $O(\varepsilon)$ of $\Omega_x = 0$, $\Omega_y = \pm 1$, respectively, and connecting the boundaries of R. The trace is negative on the part of E projecting to the right of these curves, positive to the left.

There are precisely four points where both det and tr are zero. They are located where $\Omega_x/\Omega_y = \cot 2\pi x = \pm\varepsilon$ (for outer and inner, respectively), giving two solutions x in each case, and with $y = x$ or $x + \frac{1}{2}$ respectively. These give equilibria with double eigenvalue zero. The Jordan normal form is non-diagonal because the matrix elements of (12) can not vanish simultaneously. They are Bogdanov-Takens (B) points. Thus Assumption 2 is satisfied.

We can verify the conditions for non-degeneracy of the B points. Firstly, the derivative of the map $(\mathbf{\Omega}, \mathbf{x}) \mapsto (\mathbf{G}, \mathrm{tr}, \det)$ has full rank there because the derivatives of tr and det are independent there (this implies the non-diagonal Jordan normal form, among other things). Secondly, the required conditions on the second-order Taylor coefficients of the vector field at the B point are satisfied (see Appendix B).

The part of each trace-zero curve with index $+1$ consists of centres and the trace has non-zero derivative across it so these are curves of Hopf bifurcation (possibly degenerate). The part of each trace-zero curve with index -1 consists of neutral saddles, where the eigenvalues are equal in magnitude but opposite in sign. The derivative of the trace is non-zero across it too, which will be needed later. So the trace-zero curves each consist of an arc of centre and an arc of neutral saddle.

As there are no closed curves of centre nor closed curves of neutral saddle, assumption 3a is satisfied.

On $\mathrm{tr} = 0$ we have $\cos 2\pi y = \varepsilon \sin 2\pi x$, so from (11),

$$\begin{aligned} \Omega_x &= \cos 2\pi y + \varepsilon \cos 2\pi x = \varepsilon(\sin 2\pi x + \cos 2\pi x) = \sqrt{2}\varepsilon \sin 2\pi(x + \frac{1}{8}) \\ \Omega_y &= \sin 2\pi y + \varepsilon \sin 2\pi x = \pm\sqrt{1 - \varepsilon^2 \sin^2 2\pi x} + \varepsilon \sin 2\pi x. \end{aligned} \tag{14}$$

We deduce that the trace-zero curves are mapped to simple closed curves in the parameter space close to ellipses $(\Omega_x - \Omega_y \pm 1)^2 + (\Omega_y \mp 1)^2 = \varepsilon^2$ as in Figure 24(b). They have width $2^{3/2}\varepsilon$ in Ω_x. In particular there is no simultaneous centre and neutral saddle, proving that assumption 3b holds.

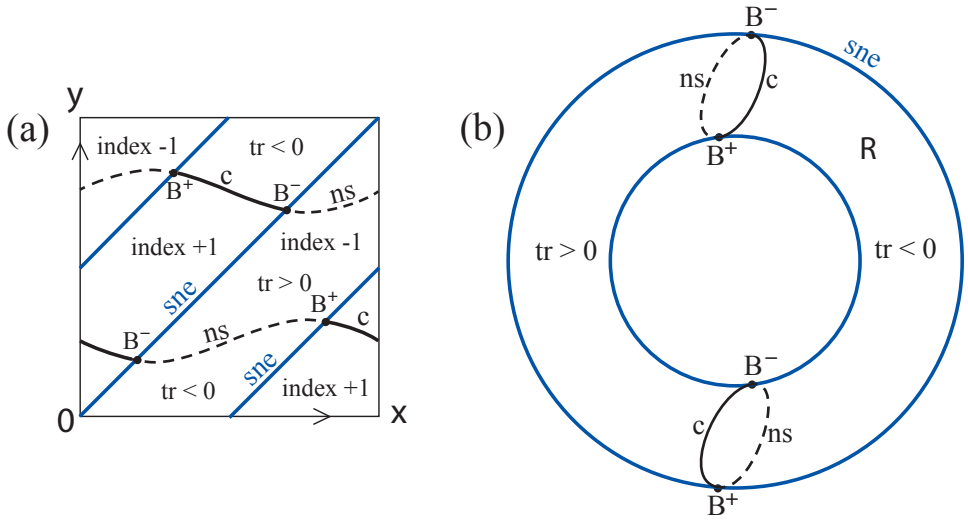

FIGURE 24. Sketch of bifurcation diagram for the equilibria of example (3) on (a) state space, (b) parameter space.

2.5. **Flow outside the resonance region.** In the unbounded component of the complement of R, which we call the "outside" of R, the vector field gives Poincaré flow. This is because if we let

$$f = \Omega_x x + \Omega_y y$$

(on the universal cover $\mathbb{R}^2$ of $\mathbb{T}^2$) and write $\Omega_x = |\mathbf{\Omega}| \cos\theta$, $\Omega_y = |\mathbf{\Omega}| \sin\theta$, then

$$\dot{f} = |\mathbf{\Omega}|^2 - |\mathbf{\Omega}| \left(\cos(2\pi y - \theta) + \varepsilon \cos(2\pi x - \theta)\right) > 0, \tag{15}$$

because $|\mathbf{\Omega}| > 1 + \varepsilon$. We can deform f slightly to $\tilde{f}$ with rational ratio of coefficients, preserving $\dot{\tilde{f}} > 0$. Then $\tilde{f} = 0$ gives a global cross-section on $\mathbb{T}^2$.

In particular, there are no Reeb components for parameter values outside the resonance region, thus satisfying Assumption 4c.

Unbounded orbits of the lift of a vector field on a torus to the plane have a "homology direction", which can be represented by the unit vector in the direction of the average velocity. For a Poincaré flow, all the orbits are unbounded and have the same homology direction.

For $\Omega_y > 1 + \varepsilon$ then $\dot{y} > 0$ so the homology direction is in the upper half circle.

For $\Omega_y > 1$, the homology direction is approximately the unit vector in the direction of $(\int_0^1 \frac{\Omega_x - \cos 2\pi y}{\Omega_y - \sin 2\pi y}\, dy, 1)$, being the value for the case $\varepsilon = 0$:

$$\begin{aligned} \dot{x} &= \Omega_x - \cos 2\pi y \\ \dot{y} &= \Omega_y - \sin 2\pi y, \end{aligned} \tag{16}$$

2.6. **Flow in $|\Omega_y| < 1-\delta$.** Next we examine the flow for parameters in a strip $|\Omega_y| < 1-\delta$ with $\delta = K\varepsilon$ for large enough K.

In this strip we can deduce a lot from the case $\varepsilon = 0$ (16), even though its resonance region degenerates to the circle $|\Omega| = 1$. It has two invariant circles at the two roots of $\sin 2\pi y = \Omega_y$. The one with $|y| < \frac{1}{4}$ is linearly attracting; the one with $|y - \frac{1}{2}| < \frac{1}{4}$ is linearly repelling (the rates are $-2\pi \cos 2\pi y = \mp 2\pi\sqrt{1-\Omega_y^2}$, which exceed $2\pi\sqrt{\delta}$ in magnitude). On the repelling one, $\dot{x} = \Omega_x + \sqrt{1-\Omega_y^2}$. Without loss of generality, take $\Omega_x \geq 0$. Then $\dot{x} > 0$ on the repelling invariant circle, so it is a right-going periodic orbit. On the attracting invariant circle, $\dot{x} = \Omega_x - \sqrt{1-\Omega_y^2}$, so it is a left-going periodic orbit for parameter values in the "hole" (the bounded component of the complement of R) and a right-going periodic orbit outside the resonance region.

By normal hyperbolicity, the invariant circles persist for small ε if K is chosen large enough. Thus in the hole and outside the resonance, for $|\Omega_y| < 1 - \delta$ we have two periodic orbits qualitatively the same as for $\varepsilon = 0$, and the rest of the flow goes from the repelling one to the attracting one, forming Reeb components in the hole and horizontal Poincaré flow outside, leftwards on the left and rightwards on the right. In the resonance region R for $\Omega_x \geq 0$ we have the repelling right-going periodic orbit and an attracting C^1 invariant circle, which must contain the two equilibria because the vector field has non-zero vertical component away from the invariant circles and the invariant circles are the unique invariant set for a neighbourhood; the rest of the flow goes from the repeller to the attractor. The saddle-node at the inner boundary splits into a saddle to the left of a node on moving towards the outer boundary; they move roughly half a revolution in opposite directions to meet again as a saddle-node at the other boundary. The directions of revolution correspond to the horizontal homotopy class of section 2.3. On the left-hand side, we have an attracting left-going periodic orbit and a repelling C^1 invariant circle containing the two equilibria. On the boundaries of the resonance we have a snic for $|\Omega_y| < 1 - \delta$. We show phase portraits in Figure 25. We label the snics with $\pm$ according to the direction of the periodic orbit they create.

To make the transition along the sne curves from the B points to the arcs of snic, there must be Z (saddle-node loop) points. To analyse this and also the whole of the flow in the parts of the hole and resonance region with $|\Omega_y| \geq 1 - \delta$, we will study this region of parameter space next.

2.7. **Flow in $|\Omega_x| \leq \sqrt{\delta}$,$|\Omega_y \mp 1| \leq \delta$.** We analyse the case near $\mathbf{\Omega} = (0, +1)$, the other one being directly analogous. The region under study is shown in Figure 26.

Write

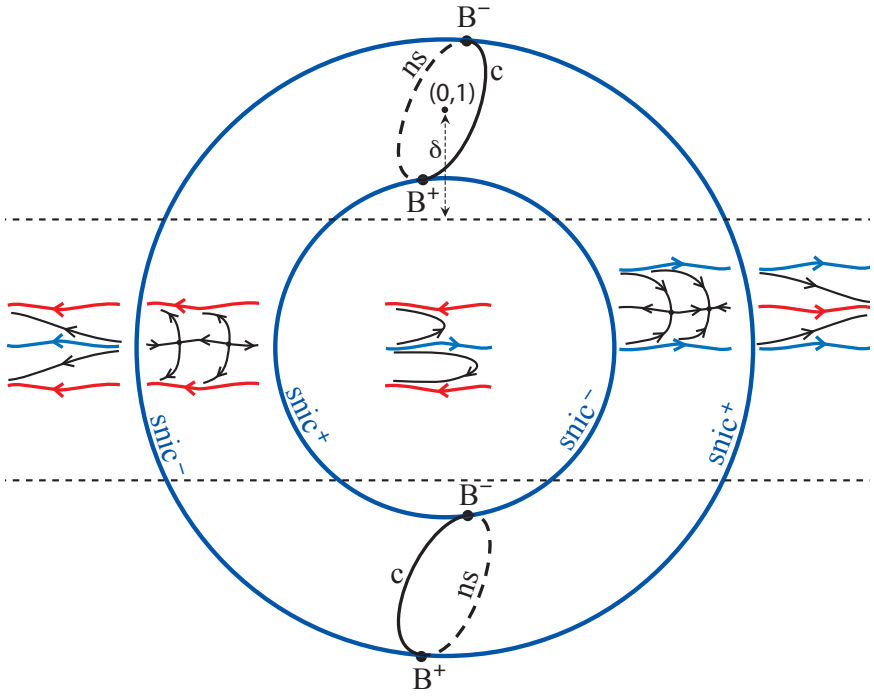

FIGURE 25. Phase portraits for parameter values in the strip $|\Omega_y| < 1 - \delta$.

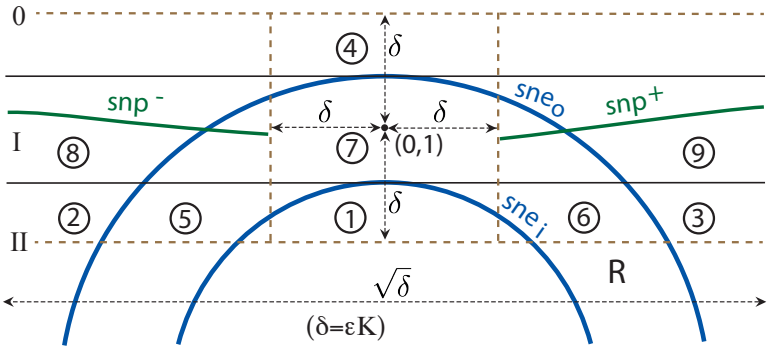

FIGURE 26. Decomposition of the $\mathbf{\Omega}$ plane near $(0, 1)$ according to number of equilibria and number of components (0, I, II) of η'-nullcline, with labels for nine sub-regions; also showing partial curves of saddle-node of periodic orbit that are deduced to exist later in section 2.7.

(17)
$$\begin{aligned} \Omega_x &= |\mathbf{\Omega}| \cos\theta \\ \Omega_y &= |\mathbf{\Omega}| \sin\theta \\ |\mathbf{\Omega}| &= 1 + \varepsilon\rho \end{aligned}$$

(so the resonance region is $|\rho| \leq 1$), and

$$\theta = \frac{\pi}{2} - 2\pi\sqrt{\varepsilon}\alpha$$

(so the top of the resonance has $\alpha = O(1)$). Away from $y = \frac{1}{4}$ then $\dot{y} > 0$ so it remains to analyse a neighbourhood of $y = \frac{1}{4}$, where the motion is slow. Write

$$y = \frac{1}{4} + \sqrt{\varepsilon}\eta$$

(so the equilibria are near $\eta = 0$), $t = s/\sqrt{\varepsilon}$, and use $'$ for d/ds. Then

$$\begin{aligned} x' &= \frac{2}{\sqrt{\varepsilon}} \sin \pi\sqrt{\varepsilon}(\eta+\alpha) \cos \pi\sqrt{\varepsilon}(\eta-\alpha) + \sqrt{\varepsilon}(\rho \sin 2\pi\sqrt{\varepsilon}\alpha - \cos 2\pi x) \\ \eta' &= \frac{2}{\varepsilon} \sin \pi\sqrt{\varepsilon}(\eta+\alpha) \sin \pi\sqrt{\varepsilon}(\eta-\alpha) + \rho \cos 2\pi\sqrt{\varepsilon}\alpha - \sin 2\pi x. \end{aligned}$$

So

$$\begin{aligned} x' &= 2\pi(\eta+\alpha) + O(\sqrt{\varepsilon}) \\ \eta' &= 2\pi^2(\eta^2 - \alpha^2) + \rho - \sin 2\pi x + O(\varepsilon). \end{aligned} \tag{18}$$

We analyse the zeroth order part of this:

$$\begin{aligned} x' &= 2\pi(\eta+\alpha) \\ \eta' &= 2\pi^2(\eta^2 - \alpha^2) + \rho - \sin 2\pi x. \end{aligned} \tag{19}$$

and then show that the remainder terms make no qualitative difference to our conclusions.

The x'-nullcline for (19) is $\eta = -\alpha$, and the η'-nullcline can be written as

$$\eta^2 = \alpha^2 + \frac{1}{2\pi^2}(\sin 2\pi x - \rho). \tag{20}$$

The latter is empty (0) for $2\pi^2\alpha^2 < \rho - 1$ (which corresponds to a region above the top of the resonance), consists of one contractible closed curve (I) for $\rho - 1 < 2\pi^2\alpha^2 < \rho + 1$ and two rotational closed curves (II) for $2\pi^2\alpha^2 > \rho + 1$. We sketch these three regions relative to the resonance region R in Figure 26, in $\mathbf{\Omega}$ coordinates, and label the subregions into which they are subdivided by R.

First, we treat parameter values in the hole (subregion 1). So $\rho < -1$. It follows that the η'-nullclines are two rotational curves. Furthermore, one is in $\eta < -|\alpha|$, the other in $\eta > |\alpha|$. The trace of the derivative of the vector field is $4\pi^2\eta$, so trace-zero is the curve $\eta = 0$. The time-derivative of the trace under the flow is

$$4\pi^2 \left(2\pi^2(\eta^2 - \alpha^2) + \rho - \sin 2\pi x\right),$$

which is negative on $\eta = 0$, because $\rho < -1$. It follows that there is a unique repelling right-going periodic orbit above $\eta = |\alpha|$ and a unique attracting left-going one under $\eta = -|\alpha|$ and the flow between them forms a Reeb component, as shown in Figure 27.

This conclusion is robust to addition of the remainder terms for ε small enough because Figure 27 is structurally stable. Thus, combining with the results of the previous section and doing the same for the bottom of the hole, we have shown that for all parameter values in the hole, the flow consists of precisely two Reeb components. This proves that our example satisfies Assumption 4a and 4b.

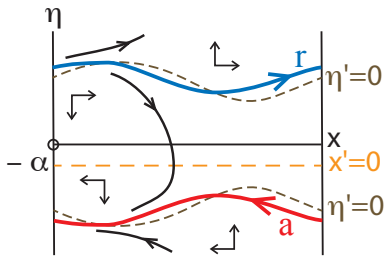

FIGURE 27. Phase portrait in sub-region 1, deduced from the indicated nullclines (dashed) and the signs of trace.

In the sub-region 2 defined by $1 < \rho < 2\pi^2\alpha^2 - 1$ and $\alpha < 0$, the phase portrait looks like Figure 28. A similar analysis to the above gives left-going attracting and repelling periodic orbits with all other orbits going from the repelling to the attracting one. Similarly in the sub-region 3 defined by $1 < \rho < 2\pi^2\alpha^2 - 1$ and $\alpha > 0$, the flow is right-going Poincaré flow with one attracting and one repelling periodic orbit.

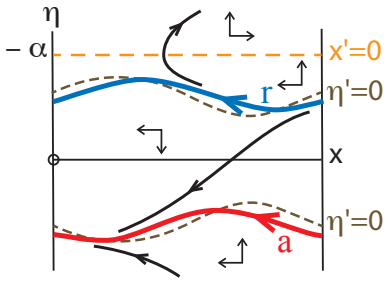

FIGURE 28. Phase portrait in sub-region 2, deduced from the indicated nullclines (dashed) and the signs of trace.

Next, in the sub-region 4 defined by $\rho > 1 + 2\pi^2\alpha^2$, the vector field has $\eta' > 0$ everywhere so there are no periodic orbits of horizontal homotopy type (we can alternatively derive this for $\Omega_y > 1 + \varepsilon$ for the exact vector field). Thus the horizontal periodic orbits of sub-regions 2 and 3 must be destroyed somewhere on traversing sub-regions 8 and 9. Generically this implies two curves of saddle-node of periodic orbits in sub-regions 8 and 9 respectively, as indicated in Figure 26, possibly with cusp points and self-intersections though they would imply regions with more than two horizontal periodic orbits; we did not rule this out but consider it unlikely.

The same approximation (19) enables us to treat parameter values in the resonance region (sub-regions 5, 6 and 7). It is convenient then to write

$$\eta = \tilde{\eta} - \alpha,$$

which puts the equilibria of (19) on $\tilde{\eta} = 0$ and fixes them for given ρ (at the roots of $\sin 2\pi x = \rho$). It yields

$$\begin{aligned} x' &= 2\pi\tilde{\eta} \\ \tilde{\eta}' &= 2\pi^2\tilde{\eta}(\tilde{\eta} - 2\alpha) + \rho - \sin 2\pi x. \end{aligned} \tag{21}$$

The saddle point (for $|\rho| < 1$) is at $\tilde{\eta} = 0, \sin 2\pi x = \rho$, with $x \in (\frac{1}{4}, \frac{3}{4})$. For given $|\rho| < 1$, the nullclines, saddle and the beginnings of its invariant manifolds are sketched for a sequence of values of α in Figure 29.

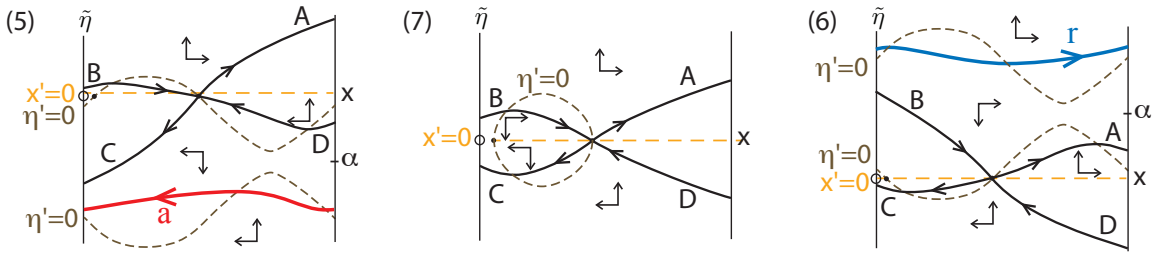

FIGURE 29. Nullclines, saddle and its branches A,B,C and D of invariant manifold, for the reduced vector field (21) for fixed $\rho \in (-1, +1)$ and α (a) large negative in sub-region 5, (b) zero in sub-region 7, (c) large positive in sub-region 6.

The slope

$$\frac{d\tilde{\eta}}{dx} = \pi(\tilde{\eta} - 2\alpha) + \frac{\rho - \sin 2\pi x}{2\pi\tilde{\eta}} \tag{22}$$

of the vector field decreases monotonically as α increases, for ρ fixed. So as α increases from large negative to large positive values, the branch A of unstable manifold of the saddle transitions from passing above B to below B, via a rotational homoclinic connection of type rhc_a^+ ($\pm$ indicates right going / left going; a/b indicates that the angle less than π in the rhc at the saddle is above / below the rhc) at a unique value $\alpha^+(\rho)$, which furthermore depends smoothly on ρ. The conclusion is robust to addition of the remainder terms for small ε.

Similarly, branch C transitions from passing below D to above D, via an rhc_b^-, at a unique value $\alpha^-(\rho)$ varying smoothly with ρ.

There can be no rhc of horizontal homotopy type for $|\Omega_y| < 1 - \delta$, because a rhc to a saddle is a non-C^1 invariant circle, contradicting the result of section 2.6. So combining the top of the resonance with the bottom, we have established that there are precisely four curves of rhc, thus satisfying Assumption 5c.

Because the slope of the vector field varies at non-zero rate with α, the homoclinic bifurcations at the curves of rhc are generic. They produce a horizontal periodic orbit which is attracting or repelling according as the trace at the saddle is negative or positive. The case where a curve of rhc crosses a curve of neutral saddle transversely produces the generic codimension-two case with a curve of saddle-node of periodic orbit (because we showed in section 2.4 that the trace has non-zero derivative across the curves of neutral saddle).

The above argument for $|\rho| < 1$ extends to the cases $\rho = \pm 1$ where the saddle is replaced by a saddle-node, giving precisely two Z points on each of the inner and outer saddle-node curves in the top. The same holds for the bottom, so justifying Assumptions 5a and 5b.

We can be more precise. The order of events on the inner sne curve going clockwise is Z^+, B, Z^-, and the order of events on the outer sne curve going clockwise is $Z^-, snp^-, B, snp^+, Z^+$. This follows from drawing phase portraits for large positive and negative α and $\alpha = 0$ (B point) on $\rho = \pm 1$ and working out which of the two rays to the B point become the ray of the saddle-node for the two signs of α. See Figure 30.

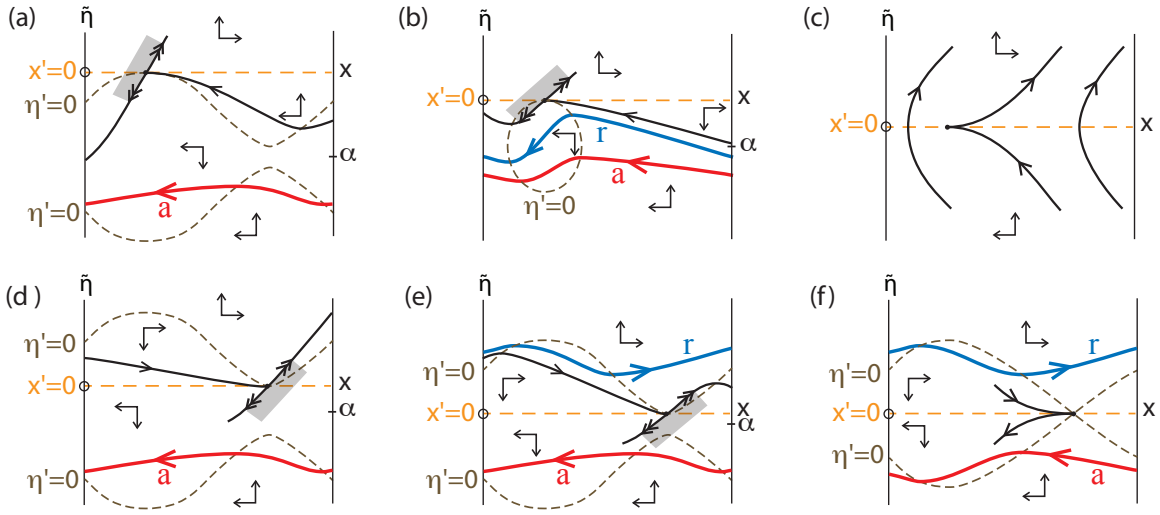

FIGURE 30. Phase portraits implying a Z^- point on the outer sne left of its B point, and a Z^+ point on the inner sne left of its B point: (a) large negative α on the outer sne, (b) negative α nearer the outer B point, (c) at the outer B point, (d) large negative α on the inner sne, (e) negative α nearer the inner B point, (f) at the inner B point.

In particular, the two curves of rhc must cross. Such an intersection is a necklace point N. We would have liked to show that $\alpha^\pm$ are monotone in ρ, making the necklace point unique in the top, but it was not obvious how to do that, so we will derive the uniqueness of N in a different way in section 2.8.2.

System (21) is symmetric under simultaneous change of sign of $\alpha, \tilde{\eta}$ and s. Thus its bifurcation diagram is symmetric under change of sign of Ω_x. The rhc curves are graphs over ρ. So the N point (or points) are on $\alpha = 0$.

Again the conclusions persist qualitatively on adding the remainder terms. In particular, the effects of the remainder terms move the N point by order $\sqrt{\varepsilon}$ in α (order ε in Ω_x).

The results are sketched in Figure 31, assuming monotonicity of $\alpha^\pm$ for simplicity.

Lastly we focus on sub-region 7. So far we have shown curves of rhc and a necklace point. If we exclude a δ-neighbourhood of $(0, 1)$, whose study is deferred to the next section, then the effects of the remainder terms in (18) are negligible. So take $\alpha \in (\frac{K}{2\pi}\sqrt{\varepsilon}, M)$, where M is sufficiently large to cover all the righthand part of sub-region 7 (α negative is similar). Vary ρ from $2\pi^2\alpha^2 - 1$ (where the η'-nullcline forms a necklace) to $2\pi^2\alpha^2 + 1$ (where the η'-nullcine shrinks to a point). The sequence of events is firstly an rhc_b^- absorbing the attracting left-going periodic orbit (unless this already happened

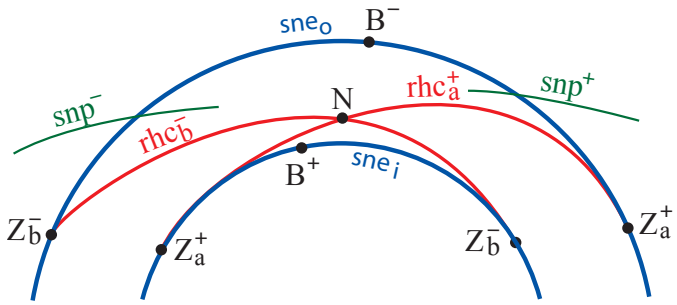

FIGURE 31. Curves of rotational homoclinic connection, Z points and necklace point N, at the top of the resonance region.

for smaller ρ), then an rhc_a^+ creating an attracting right-going periodic orbit (unless this already happened for smaller ρ). As the η'-nullcline shrinks to a point, there can no longer be any horizontal periodic orbits, as indicated in Figure 32. Thus the attracting right-going periodic orbit must saddle-node with the repelling right-going one that was left over from the Reeb flow in the hole. In conclusion the curves of snp found in sub-regions 8 and 9, continue into sub-region 7 at least up to the δ-neighbourhood of $(0,1)$, as shown in Figure 26, and there are no other bifurcations in the parts of sub-region 7 outside the δ-neighbourhood of $(0,1)$.

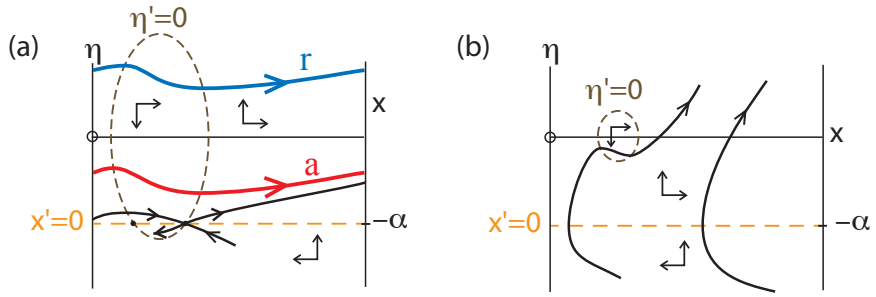

FIGURE 32. Some phase portraits for fixed $\alpha \in (\frac{K}{2\pi}\sqrt{\varepsilon}, M)$ as ρ increases: (a) just above the rhc_a^+, (b) just below the extinction of the η'-nullcline.

2.8. **δ-neighbourhood of $(0,1)$.** To complete our analysis of the vector field, we zoom in on a δ-neighbourhood of $\Omega = (0,1)$.

Here we derive an approximation for the vector field which is reversible (conjugate to its time-reverse). We use the remainder terms to prove for small $\varepsilon > 0$ that there is a unique necklace (N) point, the curves of rhc cross the curve of neutral saddle in precisely two K points, there is a unique H point, and the N point is connected to the B points by arcs of contractible homoclinic connection (chc).

2.8.1. *Reversible approximation.* We specialise the approximation (18) to a δ-neighbourhood of $\mathbf{\Omega} = (0,1)$ by putting $\alpha = \sqrt{\varepsilon}\tilde{\alpha}/2\pi$. The exact vector field is

$$\begin{aligned} x' &= \frac{2}{\sqrt{\varepsilon}} \sin(\pi\sqrt{\varepsilon}\eta + \varepsilon\tilde{\alpha}/2)\cos(\pi\sqrt{\varepsilon}\eta - \varepsilon\tilde{\alpha}/2) + \sqrt{\varepsilon}(\rho \sin\varepsilon\tilde{\alpha} - \cos 2\pi x) \\ \eta' &= \frac{2}{\varepsilon} \sin(\pi\sqrt{\varepsilon}\eta + \varepsilon\tilde{\alpha}/2)\sin(\pi\sqrt{\varepsilon}\eta - \varepsilon\tilde{\alpha}/2) + \rho\cos\varepsilon\tilde{\alpha} - \sin 2\pi x. \end{aligned} \tag{23}$$

This leads to

$$\begin{aligned} x' &= 2\pi\eta + \sqrt{\varepsilon}(\tilde{\alpha} - \cos 2\pi x) + O(\varepsilon) \\ \eta' &= 2\pi^2\eta^2 + \rho - \sin 2\pi x + O(\varepsilon). \end{aligned} \tag{24}$$

The case $\varepsilon = 0$

$$\begin{aligned} x' &= 2\pi\eta \\ \eta' &= \rho - \sin 2\pi x + 2\pi^2\eta^2 \end{aligned} \tag{25}$$

is a family of reversible vector fields with respect to the reflection $\eta \mapsto -\eta$, with one parameter ρ. We denote it by v_ρ.

On the universal cover, it is Hamiltonian with respect to the symplectic form

$$\tilde{\omega} = e^{-2\pi x} dx \wedge d\eta. \tag{26}$$

Note this 2-form is indeed closed because it can be written as $dz \wedge d\eta$ with $z = -\frac{1}{2\pi}e^{-2\pi x}$, which even makes it canonical. We found this preserved symplectic form by considering the equation for growth of ω, the ordinary area $dx \wedge d\eta$ spanned by a pair of tangent orbits:

$$\omega' = 4\pi^2\eta\omega, \tag{27}$$

which comes from taking the trace of the derivative of the vector field. From (25), this implies that

$$\frac{d\omega}{dx} = 2\pi\omega \tag{28}$$

along trajectories and so $\omega = \omega_0 e^{2\pi x}$ where ω_0 is a function of trajectory, suggesting the choice (26).

The Hamiltonian is

$$H = e^{-2\pi x}\left(\pi\eta^2 + \frac{\rho}{2\pi} - \frac{1}{4\pi}g(x)\right), \tag{29}$$

where

$$g(x) = \cos 2\pi x + \sin 2\pi x = \sqrt{2}\cos 2\pi(x - \frac{1}{8}). \tag{30}$$

H was found by solving Hamilton's equations for H with the given symplectic form:

$$\begin{aligned} e^{-2\pi x}x' &= H_\eta \\ e^{-2\pi x}\eta' &= -H_x. \end{aligned} \tag{31}$$

As for all autonomous Hamiltonian systems, H is conserved along the trajectories.

The parameter value $\rho_0 = -1/\sqrt{2}$ separates the phase portraits into the cases shown in Figure 33. This is found by considering the level sets for the saddles, as follows.

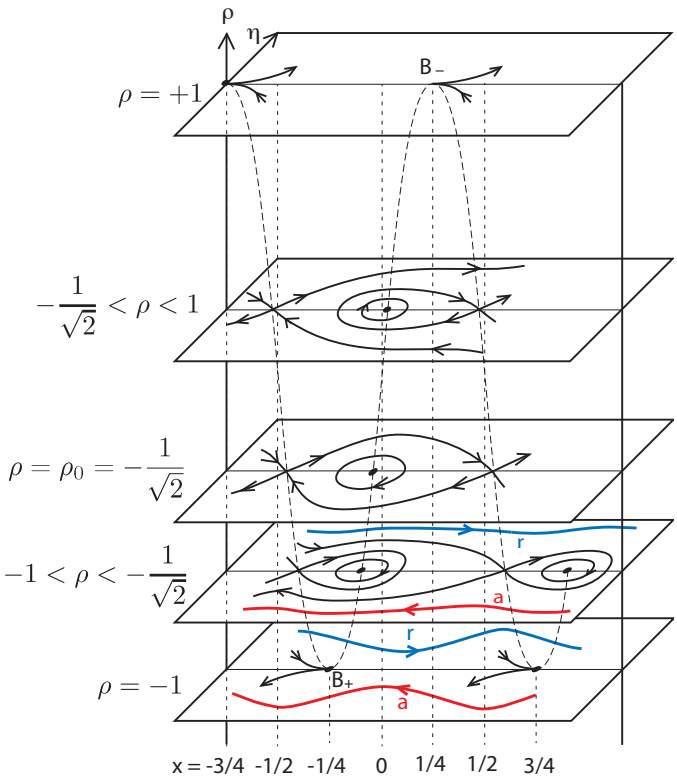

FIGURE 33. Phase portraits for the reversible family of vector fields (25) at selected values of ρ. To increase visibility, the ρ-axis has been distorted, and so have the phase portraits for $\rho = \rho_0$ and $\rho \in (-1, \rho_0)$ (the equilibria for ρ_0 are actually at $-\frac{3}{8}, -\frac{1}{8}, \frac{5}{8}$).

The equilibria are at $\eta = 0$ and the solutions x_0 of $\rho = \sin 2\pi x_0$. The solutions with $\frac{1}{4} < x_0 < \frac{3}{4} \mod 1$ are saddles. The "energy" (value of H) at an equilibrium x_0 is

$$E = \frac{1}{4\pi} e^{-2\pi x_0} (\sin 2\pi x_0 - \cos 2\pi x_0). \tag{32}$$

Its level set is

$$4\pi^2 \eta^2 = g(x) - 2 \sin 2\pi x_0 + e^{2\pi(x-x_0)} (\sin 2\pi x_0 - \cos 2\pi x_0). \tag{33}$$

From (32), the only way two saddles x_0 and $x_0 + 1$ can be at the same energy is if $\sin 2\pi x_0 = \cos 2\pi x_0$, thus $x_0 = \frac{5}{8} \mod 1$ and so $\rho = \rho_0 = -1/\sqrt{2}$ (the other solution $x_0 = \frac{1}{8}$ is a centre). The level set forms a necklace for $\rho = \rho_0$:

$$4\pi^2 \eta^2 = \sqrt{2} + g(x) = 2\sqrt{2} \cos^2 \pi (x - \frac{1}{8}), \tag{34}$$

so

$$\eta = \pm \frac{1}{\pi 2^{1/4}} \cos \pi (x - \frac{1}{8}).$$

For $\rho \in (-1, \rho_0)$ the level set includes a contractible homoclinic loop to the right. For $\rho \in (\rho_0, 1)$ it includes a contractible homoclinic loop to the left. The contractible homoclinic loops bound a region foliated by contractible periodic orbits around the centre.

Note that, despite its Hamiltonian nature on the universal cover, the vector field has an attracting periodic orbit and a repelling periodic orbit on the cylinder for $\rho < \rho_0$. Indeed the level set with $H = 0$ is invariant under $x \mapsto x + 1$, giving the periodic orbits explicitly as

$$2\pi\eta = \pm\sqrt{g(x) - 2\rho}. \tag{35}$$

Using equation (28), they have Lyapunov multipliers $e^{\pm 2\pi}$ respectively. The square of (35) also gives a periodic orbit for $\rho \in (\rho_0, 1)$ but it is contractible and neutrally stable and is just one of the continuum of such.

We now use Pontryagin's energy balance method to determine to where various features of the reversible approximation persist on adding the correction terms.

2.8.2. *Rotational homoclinic connections and necklace point.* First we consider the rotational homoclinic connections $\mathrm{rhc}^{\pm}$ from ρ_0. It is convenient to allow for an order $\sqrt{\varepsilon}$ change in ρ by setting

$$\rho = \rho_0 + \sqrt{\varepsilon}\tilde{\rho}$$

in addition to the leading correction in (24).

In Pontryagin's method one evaluates

$$\Delta H = \int_\gamma dH(\tilde{v})\ ds \tag{36}$$

along an orbit γ of the Hamiltonian vector field v_0, with $\tilde{v}$ being the first order correction to the vector field, i.e. $v = v_{\rho_0} + \sqrt{\varepsilon}\tilde{v}$, with

$$\tilde{v} = (\tilde{\alpha} - \cos 2\pi x, \tilde{\rho}) \tag{37}$$

in our case. This gives to first order the change in the value of H along a trajectory of the perturbed vector field starting on or near γ. If H is single-valued and $\Delta H \neq 0$ then the orbit does not survive the perturbation. If ΔH has a non-degenerate zero (or submanifold of non-degenerate zeroes) as a function of parameters ($\tilde{\alpha}$ and $\tilde{\rho}$ in the current case) then the orbit survives along a submanifold in parameter space close to that for $\Delta H = 0$. If H is multi-valued, as here, then one has to take into account that the values at the two saddle points might differ, but the value of H that we wish to maintain is 0 and $H = 0$ is invariant under $x \mapsto x + 1$.

Now

$$\begin{aligned} \Delta H &= \int_\gamma e^{-2\pi x}\left(x'\tilde{\rho} - \eta'(\tilde{\alpha} - \cos 2\pi x)\right) ds \\ &= \tilde{\rho}\int_\gamma e^{-2\pi x} dx - \int_\gamma e^{-2\pi x}(\tilde{\alpha} - \cos 2\pi x)\ d\eta. \end{aligned} \tag{38}$$

For the rhc^+ from $x_0 = -\frac{3}{8}$ to $+\frac{5}{8}$ the first integral is

$$\int_\gamma e^{-2\pi x} dx = C := \frac{1}{2\pi} e^{3\pi/4}(1 - e^{-2\pi}) > 0. \tag{39}$$

For the other integral, we change variable of integration to x, using

$$\frac{d\eta}{dx} = -2^{-1/4}\sin\pi(x-\frac{1}{8}) \tag{40}$$

on rhc$^+$, which follows from (34). Thus on rhc$^+$,

$$\Delta H = C\tilde\rho - A\tilde\alpha + B, \tag{41}$$

where

$$\begin{aligned} A &= -\int_\gamma 2^{-1/4}e^{-2\pi x}\sin\pi(x-\frac{1}{8})\,dx = \frac{2^{-1/4}}{4\pi}e^{3\pi/4}(1-e^{-2\pi}) \\ B &= -\int_\gamma 2^{-1/4}e^{-2\pi x}\cos 2\pi x\sin\pi(x-\frac{1}{8})\,dx = \frac{2^{-1/4}}{10\sqrt{2}\pi}e^{3\pi/4}(1-e^{-2\pi}). \end{aligned} \tag{42}$$

Thus the rhc$^+$ persists along

$$\tilde\rho = (A\tilde\alpha - B)/C \tag{43}$$

to leading order in $\sqrt{\varepsilon}$.

Similarly, for rhc$^-$ from $x_0 = \frac{5}{8}$ to $-\frac{3}{8}$, we obtain

$$\Delta H = -C\tilde\rho - A\tilde\alpha + B, \tag{44}$$

so it persists for

$$\tilde\rho = -(A\tilde\alpha - B)/C. \tag{45}$$

The approximate curves of rhc cross at $\tilde\rho = 0$, $\tilde\alpha = B/A = \sqrt{2}/5 \approx 0.283$, giving a necklace point, as shown in Figure 34. For reference, the approximate curves of rhc$^\pm$ cross $\tilde\alpha = 0$ at $\tilde\rho = \mp B/C = \mp\frac{1}{5}2^{-3/4}$. Justification of the rest of this figure will follow in the remainder of this sub-section.

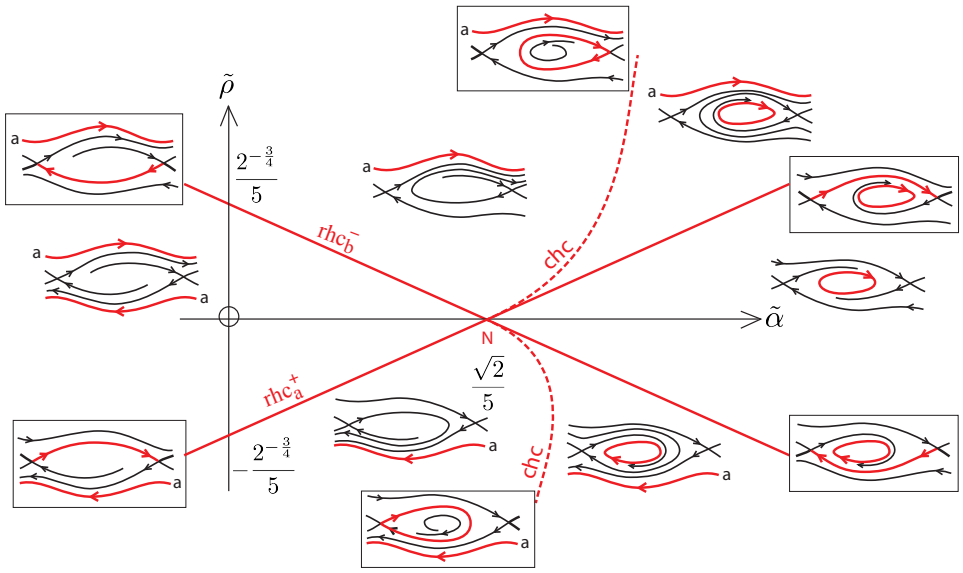

FIGURE 34. Unfolding of the necklace, with local phase portraits.

There are no other horizontal rhc in $|\rho| \leq 1, \tilde{\alpha} = O(1)$, because the phase portraits for the reversible approximation allow them only near $\rho = \rho_0$. We obtained uniqueness of $\alpha^{\pm}(\rho)$ for rhc$^{\pm}$ for $\rho \in (-1, +1)$ in section 2.7, so even if $\alpha^{\pm}$ are not monotone, there is just the one necklace point in the top of the resonance.

Doing the same for the bottom of R, this proves assumption 6.

The unfolding of a necklace point contains two arcs of contractible homoclinic bifurcation in addition to the two curves of rhc [BGKM1]. To determine the local behaviour around the necklace we need to find the sign of the trace at the saddle. To achieve that we will express the equation for zero-trace in $(\tilde{\alpha}, \rho)$ parameters, which will be useful for further purposes too.

The trace-zero loop is given to leading order in ε by the ellipse

$$\rho^2 + (\tilde{\alpha} - \rho)^2 \sim 1. \tag{46}$$

This is derived in Appendix D.

Thus the N point is to the right of the neutral saddle curve (in fact to the right of the whole trace-zero loop), as illustrated in Figure 35. Consequently the trace at the saddle at the N point is negative. This produces the unfolding of the necklace in Figure 34 (following [BGKM1]). In particular the curves of chc come in from the right.

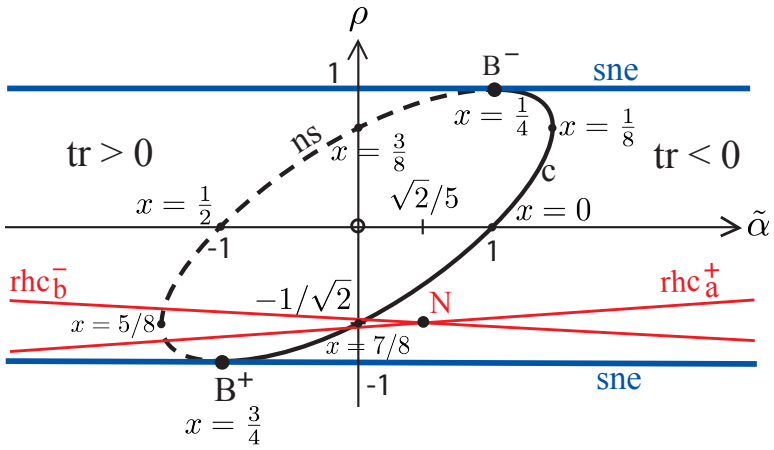

FIGURE 35. Beginning of the bifurcation diagram for (24) in $(\tilde{\alpha}, \rho)$, showing the loop of trace-zero and the curves of rhc and necklace point. For clarity, it is not drawn to scale. It also shows how the x-coordinate of the equilibrium moves round the trace-zero loop, which is needed for Appendix C.

Note that to achieve the global phase portraits near the necklace point one has to add a repelling rightwards periodic orbit above all of them (which we will do in Figure 39) and complete the phase portrait around the index +1 point (which we will discuss in Section 2.8.4).

2.8.3. *Contractible homoclinic connections.* Next we compute how the contractible homoclinic connections of the reversible approximation persist for each $\rho \in (-1, \rho_0) \cup (\rho_0, 1)$.

The saddle has level set (33). Then applying Pontryagin's method with ρ fixed this time, we obtain

$$\Delta H = -A(\rho)\tilde{\alpha} + B(\rho), \tag{47}$$

where

$$\begin{aligned} A(\rho) &= \int_\gamma e^{-2\pi x} d\eta \\ B(\rho) &= \int_\gamma e^{-2\pi x} \cos 2\pi x \; d\eta, \end{aligned} \tag{48}$$

with γ now being the chc for parameter value ρ. It is not easy to evaluate $A(\rho)$ and $B(\rho)$ but one can see that $A(\rho) > 0$ and the conclusion is that there are unique curves of chc near $\tilde{\alpha} = B(\rho)/A(\rho)$ for $\rho \in (-1, \rho_0)$ and $(\rho_0, 1)$. The chc tends to the concatenation of the two rhcs as $\rho \to \rho_0$ thus $B(\rho)/A(\rho) \to \sqrt{2}/5$ as $\rho \to \rho_0$ (the necklace point).

Indeed the unfolding of a generic N point contains two arcs of chc and we determined the directions in which they emerge in section 2.8.2.

We now show that the curves of chc tend to the B points as $\rho \to \pm 1$. To see this it is simplest to convert the integrals from line to surface integrals. We can write

$$A(\rho) = \int_{\eta_{min}}^{\eta_{max}} e^{-2\pi x_1(\eta)} - e^{-2\pi x_2(\eta)} \; d\eta,$$

with $x_1(\eta) < x_2(\eta)$ the roots of (33) on the chc. Then write the integrand as $2\pi \int_{x_1}^{x_2} e^{-2\pi x} dx$ to achieve

$$A(\rho) = 2\pi \int e^{-2\pi x} dx \; d\eta$$

over the area bounded by the chc. Similarly,

$$B(\rho) = 2\pi \int e^{-2\pi x} g(x) \; dx \; d\eta$$

over the same area. Thus $\tilde{\alpha} = B(\rho)/A(\rho)$ is the average of g over the area bounded by the chc, weighted by $e^{-2\pi x}$. As $\rho \to \pm 1$, the chc shrinks to a B point in state space and thus $\tilde{\alpha}$ tends to the value of g there. The B points have $x_0 = \pm\frac{1}{4}$ for outer/inner respectively, and thus $\tilde{\alpha} \to \pm 1$ as $\rho \to \pm 1$ which indeed correspond to the B points in parameter space. Indeed the unfolding of a non-degenerate B point contains an arc of chc, tangent to the arc of centre.

Thus the curves of chc connect the B points to the necklace point, as claimed and shown in Figure 36.

Next we prove that the curves of chc do not intersect that of ns, so there are no J points, justifying assumption 7a. From (85), the curve of neutral saddle is

$$\tilde{\alpha} \sim g(x_0),$$

taking $\rho = \sin 2\pi x_0$ with $x_0 \in (\frac{1}{4}, \frac{3}{4})$. Thus to show that the curves of chc lie to the right of the curve of ns, it is equivalent to show that the average of g over the region bounded by the chc (weighted by $e^{-2\pi x}$) is greater than the value of g at x_0. Considering the intervals of monotonicity of g, it is sufficient to show that the value of g at the extremity of the chc (i.e. where it crosses the x-axis) is greater than at the saddle. Equivalently it

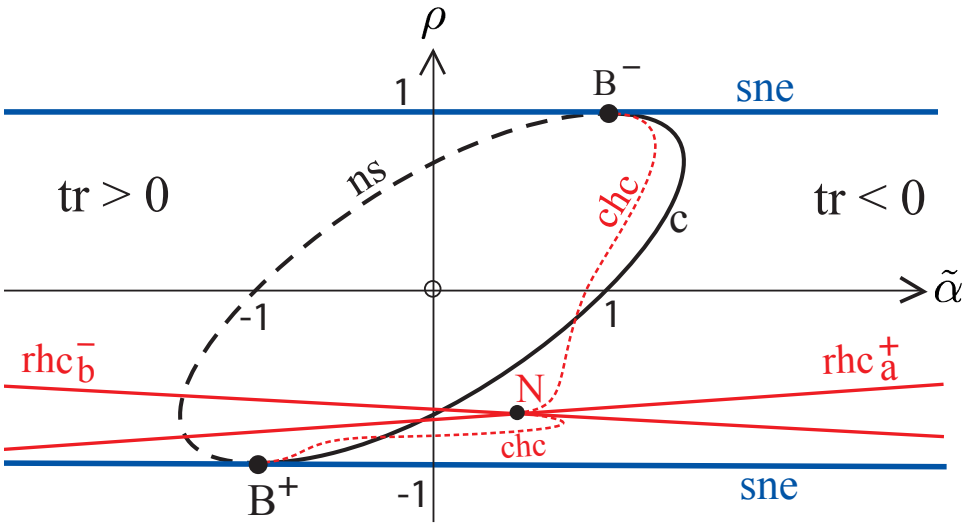

FIGURE 36. Bifurcation diagram with the addition of the curves of chc.

suffices to show that $H(x^*) > H(x_0)$ where x^* is the point with $g(x^*) = g(x_0)$ lying in $(x_0, x_0 + 1)$ if $\rho < \rho_0$ or $(x_0 - 1, x_0)$ if $\rho > \rho_0$.

For $\rho < \rho_0$ we find that $H(x^*) > H(x_0)$ iff $\cos 2\pi x_0 > \sin 2\pi x_0$ which is indeed true because $x_0 \in (-\frac{3}{8}, -\frac{1}{4})$ for this parameter interval. Similarly, for $\rho > \rho_0$ we find $H(x^*) > H(x_0)$ iff $\cos 2\pi x_0 < \sin 2\pi x_0$ which is true because $x_0 \in (\frac{1}{4}, \frac{5}{8})$ for this parameter interval. Thus there are no J points and assumption 7a is proved.

2.8.4. *Contractible periodic orbits.* Next, we would have liked to show that the contractible periodic orbits (cpos) of the reversible approximation give rise to a unique cpo for each parameter value in the zone between the curve of chc and the curve of centres. This would have proved assumption 7b (and rendered assumption 7a redundant).

There is an obvious obstacle, however: the index +1 point also has negative trace at the N point, so it is attracting, whereas all the phase portraits in Figure 34 require a repelling disc around the index +1 point. So to complete the phase portraits, the index +1 point must be surrounded by a repelling cpo throughout the whole neighbourhood. In the wedge between the arcs of chc this implies there are at least two (concentric) cpos.

Equivalently, the necklace point is outside the trace-zero loop, so the curve of chc crosses the curve of centres (above and below the necklace point). So the zone "in between" the curves of chc and centre is folded, creating a region with at least two cpos.

Another equivalent obstacle is that the first Lyapunov invariant ℓ_1 of the centre changes sign near where the curve of centres crosses the ρ and the α axes, as calculated in Appendix C, creating two points of degenerate Hopf bifurcation (D points). The first Lyapunov invariant gives the Lyapunov multiplier of the periodic orbit resulting from Hopf bifurcation, so the change in sign indicates that instead of producing an attracting periodic orbit as α decreases (as is the case near the B points) the Hopf bifurcation produces a repelling periodic orbit as α increases for parameters on the arc between the two D points. A generic D point produces an arc of saddle-node of cpo,

making a tongue with two cpos. The conjectured picture is shown in Figure 37. Note that there is a region with three (concentric) cpos and the order of nesting of the attracting and repelling cpo is different near the lower D point from near the N point, which necessitates a cusp C in the curve of csnp.

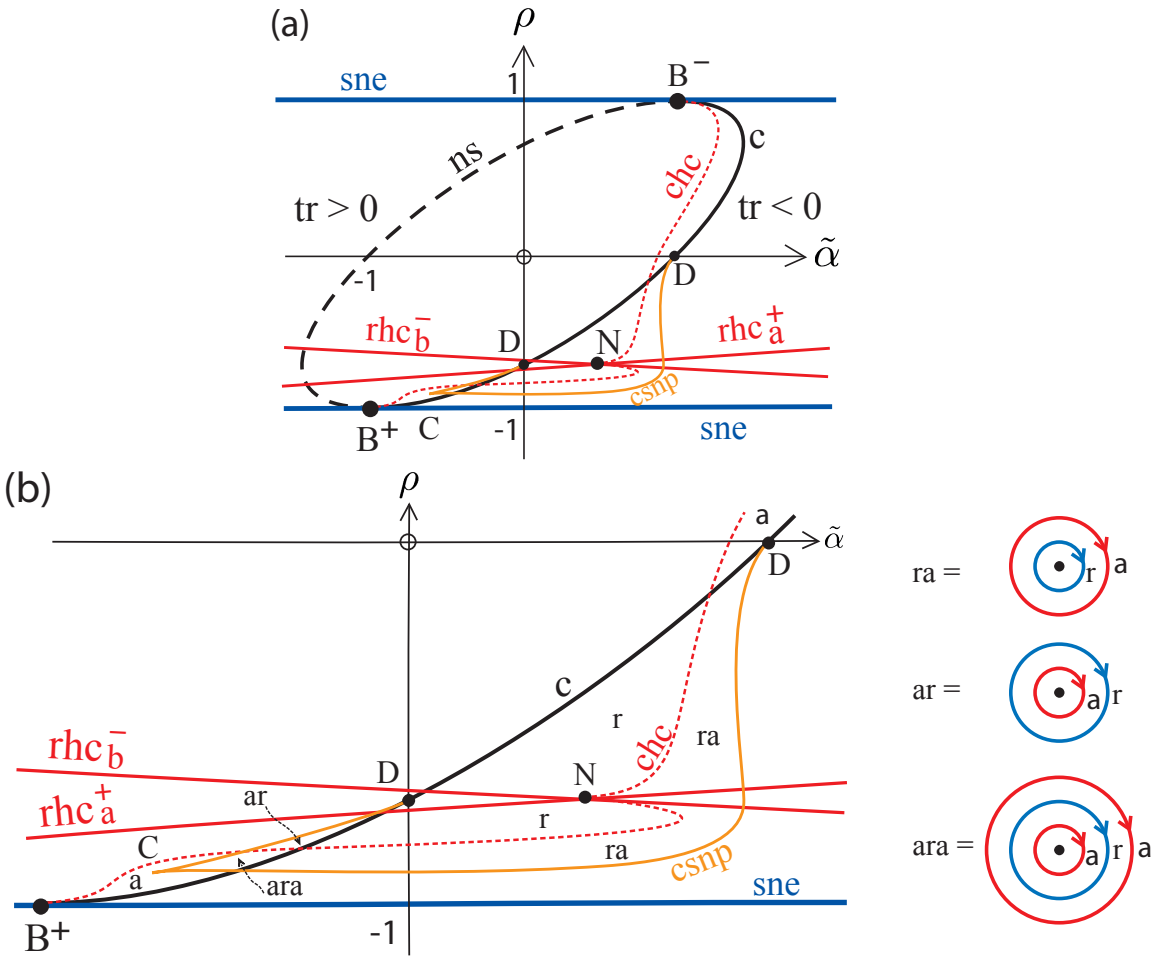

FIGURE 37. (a) Bifurcation diagram with the addition of points of degenerate Hopf bifurcation, conjectured curve of saddle-node of contractible periodic orbits (csnp). (b) Blow up of the bottom half of (a), with indication of the number and type of contractible periodic orbits.

Pontryagin's method gives a unique $\alpha(E,\rho)$ at which the periodic orbit of energy E at parameter ρ is realised to leading order in $\sqrt{\varepsilon}$. If we could do the integrals we would presumably find that α is not monotonic in E for $\rho \in (-1/\sqrt{2}, 0)$.

Nevertheless, we finish this subsection by verifying that the perturbative analysis recovers the curve of centres correctly. For a small contractible periodic orbit of (25) we can linearise $e^{-2\pi x}$ and $\cos 2\pi x\ e^{-2\pi x}$ about the centre x_0 and obtain ΔH along the

orbit to be

$$2\pi\tilde{\alpha}\ e^{-2\pi x_0}\int(x_2-x_1)\ d\eta - 2\pi g(x_0)e^{-2\pi x_0}\int(x_2-x_1)\ d\eta.$$

So this is zero on $\tilde{\alpha}=g(x_0)$, which is indeed the curve of centres for the perturbed vector field. Furthermore, the derivative with respect to $\tilde{\alpha}$ is positive, which corresponds to the trace of the index $+1$ equilibrium increasing as $\tilde{\alpha}$ is decreased. Alternatively, we could use the average over the area bounded by the periodic orbit, as in the analysis of chcs.

2.8.5. *K and H points.* Finally, we look at where the curves of $\mathrm{rhc}^{\pm}$ intersect the curve of neutral saddles, which give K points, and prove existence of resulting H points.

Because of the $\sqrt{\varepsilon}$ scaling in $\tilde{\rho}$, the curves of rhc are nearly horizontal in the plane of $(\tilde{\alpha},\rho)$. Thus they intersect the curve of neutral saddle nearly horizontally near $\rho=\rho_0$. But the curve of neutral saddle has $d\tilde{\alpha}/d\rho\sim 1-\tan 2\pi x_0=0$ at $x_0=\frac{5}{8}$, as $\varepsilon\to 0$. This comes from differentiating the equations (86,87) with respect to x. Thus the curve of neutral saddles is vertical at $\rho=\rho_0$, so the curves of rhc each intersect the curve of neutral saddle transversely and precisely once. This gives precisely two K points. This is illustrated in Figure 38. Thus assumption 8 is proved. Using (43,45), they are located near $\tilde{\alpha}=-\sqrt{2}$, $\tilde{\rho}=\mp\frac{3}{5}2^{1/4}$.

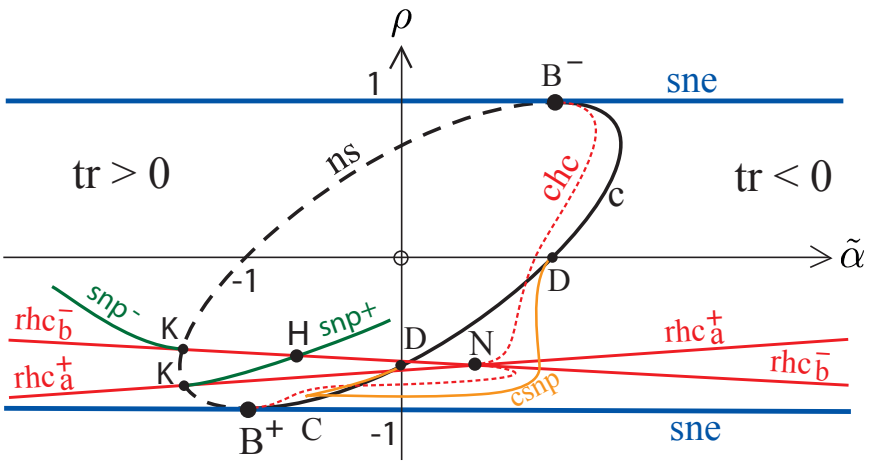

FIGURE 38. Bifurcation diagram with the addition of K points, beginnings of curves of snp, and the resulting H point.

Generically, a K point produces an arc of snp, tangent to the curve of rhc at the K point. For this example, they must occur in the directions shown in Figure 38 for compatibility with the sign of tr at the saddle, the direction in which the rhcs break and the rotational periodic orbits that exist below the necklace and not above, as illustrated in Figure 39. The arcs of snp follow closely above the curves of rhc in this δ-neighbourhood, because there are no rotational periodic orbits for the reversible approximation for $\rho\geq\rho_0$, thus they can exist only for $\rho<\rho_0+O(\sqrt{\varepsilon})$. This proves that the curve of snp^+ intersects the curve of rhc^-, giving an H point, as shown in Figure 38. The snps occur at higher order than $\sqrt{\varepsilon}$ thus the curve of snp^+ is indistinguishable to order $\sqrt{\varepsilon}$ from that

of rhc$^+$, proving uniqueness of the H point in the top. The same applies in the bottom. This proves assumption 9.

Phase portraits for the part of the bifurcation diagram involving N, K and H points are shown in Figure 39, but leaving out the complications associated with the Hopf and contractible homoclinic bifurcations.

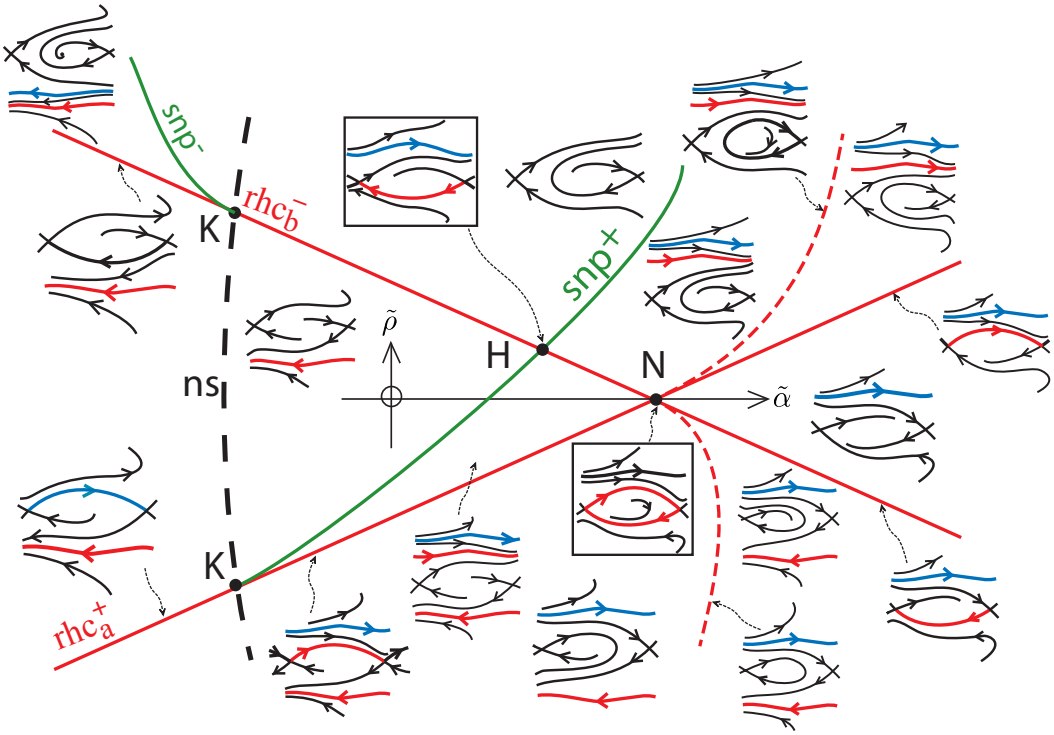

FIGURE 39. Bifurcation diagram in $(\tilde\alpha, \tilde\rho)$ coordinates around the N, K and H points, leaving out the Hopf and chc curves, showing phase portraits except near the index +1 equilibrium.

2.9. **Conclusion of Part 2.** We have made an example of a vector field satisfying all the assumptions of the Introduction except 7b.

It would be nice to confirm our conjecture about the curve of saddle-node of contractible periodic orbit, but more importantly to modify the example to achieve 7b also.

One step that is achievable is to modify the vector field near the centres to make $\ell_1 < 0$ for all of them. For example, a local perturbation which does not move the centres nor the linearisation about them but adds $-k\pi^2/f$ (in the notation of Appendix C) for some $k > \frac{1}{8}$ to ℓ_1 would make it negative for all the centres in the top of the resonance (thereby removing the D points), without changing anything outside a neighbourhood of the centre. The perturbation is only required for parameters in a neighbourhood of the curve of centres with $\ell_1 > 0$ and $1/f$ is bounded there. By choosing it to be local to a neighbourhood of the index +1 equilibrium, such a perturbation can be made without losing any of the properties already proved. But this would not satisfy assumption 7b.

Instead it would generate a closed curve of saddle-node of contractible periodic orbit around the N point.

Much better would be to explore generalisations of our example to see if the necklace point can be moved inside the trace-zero loop. If so, monotonicity of the value of α for which the periodic orbit of energy E of the reversible approximation occurs could likely be proved by Pontryagin's method, then proving assumption 7b.

We have not analysed here the fan of partial mode-locking tongues that come out of the H points. They all start with rhc boundaries (by an old private communication from Mañé). In section 1.12 we described the simplest way they interact with curves of neutral saddle, contractible homoclinic connection and saddle-node of equilibria. We presume that our example follows this simplest way, but proof would require high-order analysis for partial mode-locking type (p, q) when p or q are large.

Appendix A: At least two Hopf curves connect the boundaries of R

We are grateful to Saul Schleimer for showing us how to use the Jordan curve theorem to complete the proof of the result of section 1.5, as follows.

An *embedding* of a differentiable manifold X into a differentiable manifold Y is a differentiable map $f : X \to Y$ which is a homeomorphism onto its image and such that the derivative is one-to-one. It is *proper* if $f(\partial X) = f(X) \cap \partial Y$ and $f(X)$ is transverse to ∂Y at any point of $f(\partial X)$.

Every properly embedded closed curve in the annulus either generates the fundamental group or is null homotopic. The first type is called "essential" and the second "inessential". By the Jordan curve theorem, an inessential curve cuts a disk off the annulus and the remaining piece contains an essential curve.

Every properly embedded arc in the annulus either meets both boundary components or meets only one boundary component. Call the first type "crossing" and the second "non-crossing". By the Jordan curve theorem, a non-crossing arc cuts a disk off the annulus and the remaining piece contains an essential closed curve.

By genericity, the subset of the annulus R where the trace is zero is a finite disjoint union of properly embedded closed curves or arcs. We proved in section 1.5 that it can not contain an essential closed curve. The trace changes sign across each component of trace-zero and must return to its initial value after one revolution on the annulus, but makes an even number of sign changes for crossing each component of trace-zero other than crossing arcs, thus the number of crossing arcs is even. Suppose R contains no crossing arcs. Cut the annulus along all the inessential closed curves and the non-crossing arcs (see figure 4(d)). This leaves a component containing an essential closed curve. The trace has constant sign on it, which contradicts the result of section 1.5.

Thus there are at least two crossing arcs of trace-zero.

Appendix B: Non-degeneracy of the B points in the example

Here we prove that the B points of (3) satisfy the non-degeneracy conditions on the second-order Taylor expansion for generic bifurcation.

Following [K], we write the vector field near an equilibrium in the form

$$\mathbf{v}(\tilde{\mathbf{x}}) = A\tilde{\mathbf{x}} + \frac{1}{2}B(\tilde{\mathbf{x}}, \tilde{\mathbf{x}}) + o(|\tilde{\mathbf{x}}|^2), \tag{49}$$

where $\tilde{\mathbf{x}} = (\tilde{x}, \tilde{y})$ is the displacement from the equilibrium, A is a matrix and B is a symmetric bilinear form.

Without loss of generality, we consider the B point on the outer saddle-node curve near the top of the resonance. It has $\cot 2\pi x = \varepsilon$ with x near $\frac{1}{4}$ and $y = x$.

From (12), the derivative of the vector field is

$$DG = 2\pi \begin{bmatrix} \varepsilon \sin 2\pi x & \sin 2\pi y \\ -\varepsilon \cos 2\pi x & -\cos 2\pi y \end{bmatrix}. \tag{50}$$

So

$$A = 2\pi s \begin{bmatrix} \varepsilon & 1 \\ -\varepsilon^2 & -\varepsilon \end{bmatrix}, \tag{51}$$

where $s = \sin 2\pi x$ is near 1. Differentiating again,

$$D^2G(\tilde{\mathbf{x}}, \tilde{\mathbf{x}}') = 4\pi^2 \begin{bmatrix} \varepsilon \cos 2\pi x\ \tilde{x}\tilde{x}' + \cos 2\pi y\ \tilde{y}\tilde{y}' \\ \varepsilon \sin 2\pi x\ \tilde{x}\tilde{x}' + \sin 2\pi y\ \tilde{y}\tilde{y}' \end{bmatrix}. \tag{52}$$

So, using $\cot 2\pi x = \varepsilon$,

$$B(\tilde{\mathbf{x}}, \tilde{\mathbf{x}}') = 4\pi^2 s(\varepsilon \tilde{x}\tilde{x}' + \tilde{y}\tilde{y}') \begin{bmatrix} \varepsilon \\ 1 \end{bmatrix}. \tag{53}$$

Let

$$\mathbf{q}_0 = \begin{bmatrix} 1 \\ -\varepsilon \end{bmatrix},\ \mathbf{q}_1 = \frac{1}{1+\varepsilon^2} \begin{bmatrix} \varepsilon \\ 1 \end{bmatrix}, \tag{54}$$

being respectively a null vector of A ($A\mathbf{q}_0 = 0$) and an independent vector scaled to make $A\mathbf{q}_1 = \mathbf{q}_0$. Let

$$\mathbf{p}_1 = [\varepsilon\ 1],\ \mathbf{p}_0 = \frac{1}{1+\varepsilon^2}[1\ -\varepsilon], \tag{55}$$

being respectively a null form of A ($\mathbf{p}_1 A = 0$) scaled to make $\mathbf{p}_1\mathbf{q}_1 = 1$ (where $\mathbf{pq}$ is matrix multiplication), and a form $\mathbf{p}_0$ chosen so that $\mathbf{p}_0\mathbf{q}_1 = 0$ and scaled to make $\mathbf{p}_0 A = \mathbf{p}_1$ (equivalently $\mathbf{p}_0\mathbf{q}_0 = 1$).

Then the non-degeneracy conditions for a B point are [K]

$$\begin{aligned} a &= \frac{1}{2}\mathbf{p}_1 B(\mathbf{q}_0, \mathbf{q}_0) \neq 0 \\ b &= \mathbf{p}_0 B(\mathbf{q}_0, \mathbf{q}_0) + \mathbf{p}_1 B(\mathbf{q}_0, \mathbf{q}_1) \neq 0. \end{aligned} \tag{56}$$

We compute

$$B(\mathbf{q}_0, \mathbf{q}_0) = 4\pi s^2(\varepsilon + \varepsilon^2) \begin{bmatrix} \varepsilon \\ 1 \end{bmatrix}, \tag{57}$$

so

$$a = 2\pi^2 s\varepsilon(1+\varepsilon)(1+\varepsilon^2) \neq 0 \tag{58}$$

for $\varepsilon \in (0, 1)$. Next, $\mathbf{p}_0 B(\mathbf{q}_0, \mathbf{q}_0) = 0$ but

$$\mathbf{p}_1 B(\mathbf{q}_0, \mathbf{q}_1) = 4\pi^2 s\varepsilon(\varepsilon - 1), \tag{59}$$

so $b \neq 0$.

The sign of ab gives the sign of the coefficient β in the normal form (as recalled in subsection 1.5.2), so we see that $\beta = -1$ for the top outer B point. Our frame $(\mathbf{q}_0, \mathbf{q}_1)$ is positively oriented, thus the top outer B point has Fiedler B-index -1. Similarly, the B-indices of the other B points are $(+1, -1, +1)$ in descending order, as indicated in Figure 24.

To complete this appendix we compute the curve of improper nodes. The condition is $\mathrm{tr}^2 = 4\det$. This reduces to

$$(\cos 2\pi y + \varepsilon \sin 2\pi x)^2 = 4\varepsilon \sin 2\pi y \cos 2\pi x,$$

which also gives closed curves around $\Omega_x = 0, \Omega_y = \pm 1$, through the B points. Note that they have asymptotic width $2\sqrt{\varepsilon}$ in Ω_x, much wider than for the trace-zero curves. They play a role in delimiting the region of existence of a C^1 invariant circle (cf. [BM1]).

Appendix C: Analysis of the centres in the example

Here we calculate the first Lyapunov invariant (the combination of second and third order Taylor coefficients that decides whether the centre is nonlinearly attracting or repelling) for the curve of centres for the example (3). Unfortunately, we find that it passes through zero twice along the curve of centres, creating two points of degenerate Hopf bifurcation.

We follow [K], by first finding an affine coordinate change

$$\tilde{\mathbf{x}} = \begin{bmatrix} a & b \\ c & d \end{bmatrix} \delta\mathbf{x}, \tag{60}$$

where $\delta\mathbf{x} = \mathbf{x} - \mathbf{x}_0$, with $\Delta = ad - bc \neq 0$ and inverse

$$\delta\mathbf{x} = \frac{1}{\Delta} \begin{bmatrix} d & -b \\ -c & a \end{bmatrix} \tilde{\mathbf{x}}, \tag{61}$$

to reduce the linearised dynamics around the centre $\mathbf{x}_0$ to the form

$$\dot{\tilde{x}} = A\tilde{\mathbf{x}} = \begin{bmatrix} 0 & -\omega \\ \omega & 0 \end{bmatrix} \tilde{\mathbf{x}}. \tag{62}$$

The equilibria with $\mathrm{tr} = 0$ can be parametrised by $x_0 \in \mathbb{R}$ and the choice of root y_0 of $\cos 2\pi y_0 = \varepsilon \sin 2\pi x_0$, near $\pm\frac{1}{4}$ for the top and bottom of the resonance, respectively. They are centres for $y_0 - x_0 \in (0, \frac{1}{2})$. It is enough to treat the centres in the top of the resonance, so we restrict attention to that case from now on. Thus x_0 goes from slightly above $-\frac{1}{4}$ to slightly below $+\frac{1}{4}$, the ends being the B points.

On $\mathrm{tr} = 0$, the derivative (12) in $\mathbf{x}$-coordinates has the form

$$2\pi \begin{bmatrix} \varepsilon S & \Gamma \\ -\varepsilon C & -\varepsilon S \end{bmatrix}, \tag{63}$$

where $S = \sin 2\pi x_0$, $C = \cos 2\pi x_0$, and $\Gamma = \sqrt{1 - \varepsilon^2 S^2}$ (the plus sign corresponds to the centres in the top of the resonance). The eigenvalues $\pm i\omega$ are given by

$$\omega^2 = 4\pi^2 \varepsilon(\Gamma C - \varepsilon S^2). \tag{64}$$

Note that on the curve of centres, ω^2 is positive. To simplify formulae, we write

$$\omega = 2\pi f, \quad f = \sqrt{\varepsilon(\Gamma C - \varepsilon S^2)}. \tag{65}$$

For future reference, note that $f = O(\sqrt{\varepsilon})$ and

$$\varepsilon\Gamma C = \varepsilon^2 S^2 + f^2. \tag{66}$$

The equations for the coordinate change (60) are

$$\begin{aligned} \varepsilon S(ad+bc) &= \Gamma ac + \varepsilon C bd \\ 2\varepsilon S(ab-cd) &= \Gamma(a^2-c^2) + \varepsilon C(b^2-d^2) \end{aligned} \tag{67}$$

(the first makes both the diagonal elements zero and the second makes the off-diagonal elements sum to zero). There are two dimensions of freedom (rotation and scale) in the choice of solution, but the solution we choose is

$$\begin{aligned} a = \varepsilon S(\Gamma + \varepsilon C), \qquad b = 1 \\ c = f\Gamma, \quad d = -f\varepsilon S, \end{aligned} \tag{68}$$

which can be checked to work, using the definitions of f and Γ and the relation $C^2+S^2 = 1$. Note that the positive square root in (65) achieves the correct signs in (62).

The determinant Δ of the matrix defined by (68) can be written:

$$\Delta = -f\Delta_0, \tag{69}$$

with

$$\Delta_0 = \Gamma + \varepsilon^2 S^2(\Gamma + \varepsilon C) = (1 + \varepsilon^2 S^2 f^2)/\Gamma. \tag{70}$$

Note that $\Delta_0 \to 1$ as $\varepsilon \to 0$, so $\Delta \sim -f$.

Taylor expanding the vector field (3) about the centre $\mathbf{x}_0$ to third order in $\delta\mathbf{x}$ yields

$$\begin{aligned} \dot{x} &= 2\pi(\varepsilon S\delta x + \Gamma\delta y) + 2\pi^2(\varepsilon C\delta x^2 + \varepsilon S\delta y^2) - \frac{4}{3}\pi^3(\varepsilon S\delta x^3 + \Gamma\delta y^3) \\ \dot{y} &= -2\pi(\varepsilon C\delta x + \varepsilon S\delta y) + 2\pi^2(\varepsilon S\delta x^2 + \Gamma\delta y^2) + \frac{4}{3}\pi^3(\varepsilon C\delta x^3 + \varepsilon S\delta y^3). \end{aligned} \tag{71}$$

We already designed the transformation to put the linear part into the form (62). So we write the transformed vector field to third order as

$$\dot{\tilde{x}} = A\tilde{\mathbf{x}} + \begin{bmatrix} P \\ Q \end{bmatrix}, \tag{72}$$

and compute

$$\begin{aligned} P = \quad & \tfrac{2\pi^2}{\Delta^2}\left((a\varepsilon C + b\varepsilon S)(d\tilde{x} - b\tilde{y})^2 + (a\varepsilon S + b\Gamma)(-c\tilde{x} + a\tilde{y})^2\right) \\ & + \tfrac{4\pi^3}{3\Delta^3}\left((-a\varepsilon S + b\varepsilon C)(d\tilde{x} - b\tilde{y})^3 + (-a\Gamma + b\varepsilon S)(-c\tilde{x} + a\tilde{y})^3\right). \end{aligned} \tag{73}$$

Similarly

$$\begin{aligned} Q = \quad & \tfrac{2\pi^2}{\Delta^2}\left((c\varepsilon C + d\varepsilon S)(d\tilde{x} - b\tilde{y})^2 + (c\varepsilon S + d\Gamma)(-c\tilde{x} + a\tilde{y})^2\right) \\ & + \tfrac{4\pi^3}{3\Delta^3}\left((-c\varepsilon S + d\varepsilon C)(d\tilde{x} - b\tilde{y})^3 + (-c\Gamma + d\varepsilon S)(-c\tilde{x} + a\tilde{y})^3\right). \end{aligned} \tag{74}$$

The following factors in the quadratic terms can be written as

$$\begin{aligned} aC + bS &= \varepsilon SC(\Gamma + \varepsilon C) + S = S(1 + \varepsilon^2 - f^2) \\ a\varepsilon S + b\Gamma &= \varepsilon^2 S^2(\Gamma + \varepsilon C) + \Gamma = (1 + \varepsilon^2 S^2 f^2)/\Gamma \\ cC + dS &= f\Gamma C - f\varepsilon S^2 = -f^3/\varepsilon \\ c\varepsilon S + d\Gamma &= f\Gamma\varepsilon S - f\varepsilon S\Gamma = 0. \end{aligned} \tag{75}$$

The first Lyapunov coefficient is [K]

$$\begin{aligned}\ell_1 &= \frac{1}{8\omega}(P_{xxx}+P_{xyy}+Q_{xxy}+Q_{yyy}) \\ &\quad +\frac{1}{8\omega^2}\left(P_{xy}(P_{xx}+P_{yy})-Q_{xy}(Q_{xx}+Q_{yy})-P_{xx}Q_{xx}+P_{yy}Q_{yy}\right),\end{aligned} \tag{76}$$

where we have dropped the tildes from x and y, and the derivatives are evaluated at 0.

The easiest terms are

$$\begin{aligned}Q_{xx} &= -4\pi^2 f^3\varepsilon^2 S^2/\Delta_0^2 \\ Q_{xy} &= -4\pi^2 f^2\varepsilon S/\Delta_0^2 \\ Q_{yy} &= -4\pi^2 f/\Delta_0^2.\end{aligned} \tag{77}$$

In particular

$$Q_{xy}(Q_{xx}+Q_{yy}) = 16\pi^4 f^2\varepsilon S(1+f^2\varepsilon^2 S^2)/\Delta_0^4, \tag{78}$$

which is $O(f^2\varepsilon S)$.

Next

$$\begin{aligned}P_{xx} &= \frac{4\pi^2}{\Delta_0^2}\left((1+\varepsilon^2 S^2 f^2)\Gamma+\varepsilon^3 S^3(1+\varepsilon^2-f^2)\right) \\ P_{xy} &= -\frac{4\pi^2\varepsilon S}{f\Delta_0^2}\left((1+\varepsilon^2 S^2 f^2)(\Gamma+\varepsilon C)-\varepsilon S(1+\varepsilon^2-f^2)\right) \\ P_{yy} &= \frac{4\pi^2\varepsilon S}{f^2\Delta_0^2}\left((1+\varepsilon^2 S^2 f^2)\varepsilon S(\Gamma+\varepsilon C)/\Gamma+(1+\varepsilon^2-f^2)\right).\end{aligned} \tag{79}$$

Thus $P_{xx}Q_{xx} = O(f^3\varepsilon^2 S^2)$, $P_{yy}Q_{yy}$ and $P_{xy}P_{xx}$ are $O(\varepsilon S/f)$, and $P_{xy}P_{yy} = O(\varepsilon^2 S^2/f^3)$.

Turning to the cubic terms, factors of the coefficients can be simplified as follows.

$$\begin{aligned}-aS+bC &= -\varepsilon S^2(\Gamma+\varepsilon C)+C = \Gamma f^2/\varepsilon \\ -a\Gamma+b\varepsilon S &= -\varepsilon S(\Gamma+\varepsilon C)\Gamma+\varepsilon S = -\varepsilon S f^2 \\ -cS+dC &= -f(\Gamma S+\varepsilon SC) = -fS(\Gamma+\varepsilon C) \\ -c\Gamma+d\varepsilon S &= -f(\Gamma^2+\varepsilon^2 S^2) = -f.\end{aligned} \tag{80}$$

Then

$$\begin{aligned}Q_{yyy} &= \frac{8\pi^3\varepsilon S}{f^2\Delta_0^3}(\Gamma+\varepsilon C)\left(1-\varepsilon^2 S^2(\Gamma+\varepsilon C)^2\right) \\ Q_{xxy} &= -8\pi^3\varepsilon S(\Gamma+\varepsilon C)/\Delta_0^3 \\ P_{xxx} &= 8\pi^3\varepsilon S\Gamma f^2/\Delta_0^3 \\ P_{xyy} &= -8\pi^3\varepsilon\Gamma S\left(1-\varepsilon^2 S^2(\Gamma+\varepsilon C)^2\right)/\Delta_0^3.\end{aligned} \tag{81}$$

Combining the terms of (76),

$$\ell_1 \sim -\frac{\pi^2\varepsilon S}{2f^5}\left(f^2+\varepsilon S+O(\varepsilon^2)\right). \tag{82}$$

So $\ell_1 \neq 0$ except when $S=0$, which happens where the curve of centres crosses $\rho=0$ ($x=0$, see Figure 35), or when $S=-f^2/\varepsilon+O(\varepsilon)$, which happens near where the curve

of centres crosses $\tilde{\alpha} = 0$ ($x = 7/8$). Indeed, using the equations for the trace-zero curve, we find the second point has $\tilde{\alpha} = O(\varepsilon)$, $\tilde{\rho} = O(\sqrt{\varepsilon})$).

Thus there are two points of degenerate Hopf bifurcation (D). A generic D point produces an arc of saddle-node of contractible periodic orbit. Presumably the D points are generic (this could be determined by proving that the second Lyapunov invariant is non-zero). If so, there is a curve of saddle-node of contractible periodic orbit joining them, because there are no other places for the arcs of csnp to go to. It must pass to the right of the necklace point to absorb the cpo created by the chcs. Given the location of the D point in the wedge between the rhcs, we conjecture that the curve of csnp is arranged as in Figure 37.

Appendix D: Trace-zero loop for the example

Equation (13) for zero-trace in the example can be written as $\sin 2\pi\sqrt{\varepsilon}\eta + \varepsilon \sin 2\pi x = 0$, which to leading order in ε says that

$$\eta = \frac{\sqrt{\varepsilon}}{2\pi} \sin 2\pi x. \tag{83}$$

The equations (11) for the equilibria as functions of parameter values can be written

$$\begin{aligned} (1+\varepsilon\rho)\sin\varepsilon\tilde{\alpha} + \sin 2\pi\sqrt{\varepsilon}\eta &= \varepsilon\cos 2\pi x \\ (1+\varepsilon\rho)\cos\varepsilon\tilde{\alpha} - \cos 2\pi\sqrt{\varepsilon}\eta &= \varepsilon\sin 2\pi x. \end{aligned} \tag{84}$$

Using trace-zero, the first equation leads to

$$\sin 2\pi x + \cos 2\pi x \sim \tilde{\alpha}, \tag{85}$$

as $\varepsilon \to 0$. The second equation can be written as

$$\sin 2\pi x = \frac{2}{\varepsilon} \sin(\pi\sqrt{\varepsilon}\eta + \varepsilon\tilde{\alpha}/2) \sin(\pi\sqrt{\varepsilon}\eta - \varepsilon\tilde{\alpha}/2) + \rho\cos\varepsilon\tilde{\alpha}.$$

So

$$\sin 2\pi x \sim 2(\pi^2\eta^2 - \varepsilon\tilde{\alpha}^2/4) + \rho \sim \rho, \tag{86}$$

because $\eta = O(\sqrt{\varepsilon})$ from (83). Putting this into (85) yields

$$\cos 2\pi x \sim \tilde{\alpha} - \rho. \tag{87}$$

Lastly, we eliminate x (the horizontal position of the trace-zero equilibrium) between (86) and (87) to obtain (46): $\rho^2 + (\tilde{\alpha} - \rho)^2 \sim 1$.

References

[AZ] Aranson S, Zhuzhoma E, Qualitative theory of flows on surfaces (a review) J Math Sci 90 (1998) 2051–2110 (translated from Itogi Nauk Tekh, Mat Prilozh 32 (1996)).

[BGKM1] Baesens C, Guckenheimer J, Kim S, MacKay RS, Three coupled oscillators: mode-locking, global bifurcations and toroidal chaos, Physica D 49 (1991) 387–475.

[BGKM2] Baesens C, Guckenheimer J, Kim S, MacKay R, Simple resonance regions of torus diffeomorphisms, in: Patterns and Dynamics in Reactive Media, eds Aris R, Aronson DG, Swinney HL (Springer, 1991), 1–9.

[BM1] Baesens C, MacKay RS, Resonances for weak coupling of the unfolding of a saddle-node periodic orbit with an oscillator, Nonlinearity 20 (2007) 1283–98.

[BM2] Baesens C, MacKay RS, Interaction of two systems with saddle-node bifurcation on invariant circle, part 1, Foundations and the mutualistic case, Nonlinearity 26 (2013) 3043–76.

[F] Fiedler B, Global Hopf bifurcation of two-parameter flows, Arch Rat Mech Anal 94 (1986) 59–81 (see also Fiedler B, An index for global Hopf bifurcation in parabolic systems, J Reine Angew Math 359 (1985) 1–36).

[G] Galkin OG, Resonance regions for Mathieu type dynamical systems on a torus, Phys D 39 (1989) 287–98.

[GGT] Gambaudo J-M, Glendinning P, Tresser C, Stable cycles with complicated structure, J Phys Lett (Paris) 46 (1985) L653–7.

[GH] Guckenheimer J, Holmes P, Nonlinear oscillations, dynamical systems and Bifurcations of vector fields (Springer, 1983).

[KH] Katok A, Hasselblatt B, Introduction to the Modern Theory of Dynamical Systems (Cambridge U Press, 1995).

[KMG] Kim S, MacKay RS, Guckenheimer J, Resonance regions for families of torus maps, Nonlinearity 2 (1989) 391–404.

[K] Kuznetsov YuA, Elements of applied bifurcation theory (Springer, 2nd edition, 1998)

[M] MacKay RS, A simple proof of Denjoy's theorem, Math Proc Cam Phil Soc 103 (1988) 299–303.

[NOB] Neumann D, O'Brien T, Global structure of continuous flows on 2-manifolds, J Diff Eq 22 (1976) 89–110.

[S] Siegel CL, Note on differential equations on the torus, Ann Math 46 (1945) 423–8.

[YM] Yamapi R, MacKay RS, Stability of synchronisation in a shift-invariant ring of mutually coupled oscillators, Discr Conts Dyn Sys B 10 (2008) 973–996.

Mathematics Institute, University of Warwick, Coventry CV4 7AL, U.K.